AD-A156 911 APPLICATION OF AN OBJECTIVE ANALYSIS SCHEME TO MESOSCALE OBSERVATIONAL NETWORK DESIGN(U) AIR FORCE INST OF TECH WRIGHT-PATTERSON AFB OH D E HARMS 1985 1/2

UNCLASSIFIED AFIT/CI/NR-85-43T F/G 12/1 NL

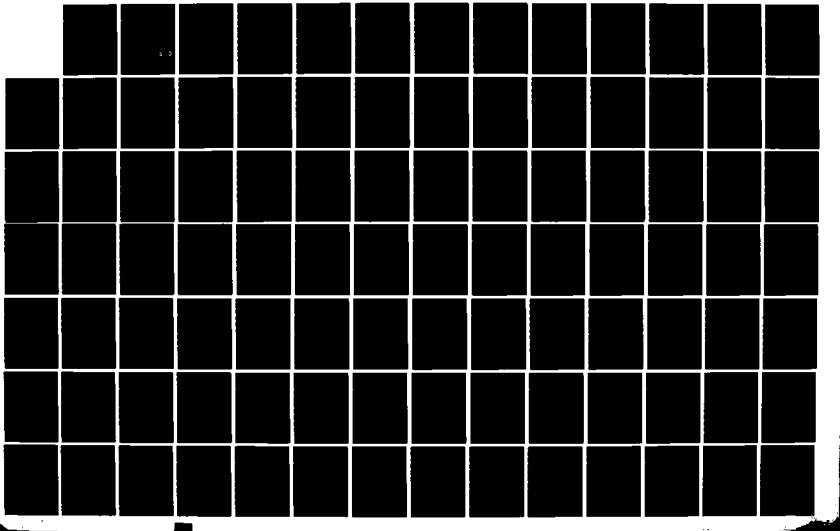

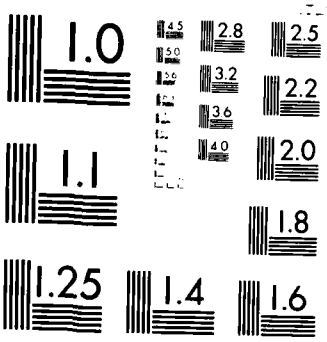

# APPLICATION OF AN OBJECTIVE ANALYSIS SCHEME TO MESOSCALE OBSERVATIONAL NETWORK DESIGN

by

DEWEY E. HARMS, Capt, USAF

A thesis submitted to the Graduate Faculty of
North Carolina State University
in partial fulfillment of the
requirements for the Degree of
Masters of Science

(Total number of pages: 97)

Raleigh

1 9 8 5

UNCLASS

SECURITY CLASSIFICATION OF THIS PAGE (When Data Entered)

| REPORT DOCUMENTATION PAGE | | READ INSTRUCTIONS BEFORE COMPLETING FORM |
|---|---|---|
| 1. REPORT NUMBER<br>AFIT/CI/NR 85-43T | 2. GOVT ACCESSION NO.<br>AD A156 711 | 3. RECIPIENT'S CATALOG NUMBER |
| 4. TITLE (and Subtitle)<br>Application Of An Objective Analysis Scheme To Mesoscale Observational Network Design | | 5. TYPE OF REPORT & PERIOD COVERED<br>THESIS/DISSERTATION |
| | | 6. PERFORMING ORG. REPORT NUMBER |
| 7. AUTHOR(s)<br>Dewey E. Harms | | 8. CONTRACT OR GRANT NUMBER(s) |
| 9. PERFORMING ORGANIZATION NAME AND ADDRESS<br>AFIT STUDENT AT: North Carolina State University | | 10. PROGRAM ELEMENT, PROJECT, TASK AREA & WORK UNIT NUMBERS |
| 11. CONTROLLING OFFICE NAME AND ADDRESS<br>AFIT/NR<br>WPAFB OH 45433 | | 12. REPORT DATE<br>1985 |
| | | 13. NUMBER OF PAGES<br>91 |
| 14. MONITORING AGENCY NAME & ADDRESS(If different from Controlling Office) | | 15. SECURITY CLASS. (of this report)<br>UNCLASS |
| | | 15a. DECLASSIFICATION/DOWNGRADING SCHEDULE |

16. DISTRIBUTION STATEMENT (of this Report)

APPROVED FOR PUBLIC RELEASE; DISTRIBUTION UNLIMITED

17. DISTRIBUTION STATEMENT (of the abstract entered in Block 20, if different from Report)

18. SUPPLEMENTARY NOTES

APPROVED FOR PUBLIC RELEASE: IAW AFR 190-1

LYNN E. WOLAVER
Dean for Research and
Professional Development
AFIT, Wright-Patterson AFB OH

19. KEY WORDS (Continue on reverse side if necessary and identify by block number)

20. ABSTRACT (Continue on reverse side if necessary and identify by block number)

ATTACHED

DD FORM 1 JAN 73 1473 EDITION OF 1 NOV 65 IS OBSOLETE

UNCLASS

SECURITY CLASSIFICATION OF THIS PAGE (When Data Entered)

## ABSTRACT

HARMS, DEWEY ELVIN. Application of an Objective Analysis Scheme to Mesoscale Observational Network Design. (Under the direction of DAVID BARBER and GERALD WATSON.)

This research program was initiated with the overall objective of estimating the probable effectiveness of the proposed surface observational network ((PAM, II) which will be deployed as part of the winter 1986 GALE field project. This network is to contribute to the study of mesoscale features within developing east coast cyclones, and especially the well-known coastal front.

To accomplish this objective, the process of spatial weighted-averaging interpolation of surface data was investigated by using the Barnes (1973) objective analysis scheme. Tests were conducted to determine the limitations of the Barnes analysis method and evaluate how well this technique reconstructs meteorological fields. A method was developed which enables an optimum weight parameter to be determined for a given data distribution.

Barnes objective analyses were generally more accurate than kinematic fields based on detailed hand analyses. The objective analysis scheme effectively filtered random errors typical of instrumental and exposure effects from the analysis. However, interpolation near the edge of a data domain and extrapolation into data void regions led to

erroneous results.

An optimum weight parameter of 500 $km^2$ was obtained in a mid-west cyclone test case. This resulted in a total response of 0.936 for wavelengths of twice the station spacing.

The Barnes objective analysis method was also used in conjunction with mathematically simulated PAM II data to estimate the probable analysis accuracy of the system (analysis plus network). Analyses based on the present PAM II network design did not adequately represent the true meteorological field containing mesoscale structure. Percentage errors exceeded 100% in the case of temperature advection and local frontogenesis. However, the proposed PAM II network provided analyses nearly as good as those using a twice as dense network, and somewhat better than those obtained using the regular hourly reporting stations.

ABSTRACT

HARMS, DEWEY ELVIN. Application of an Objective Analysis Scheme to Mesoscale Observational Network Design. (Under the direction of DAVID BARBER and GERALD WATSON.)

This research program was initiated with the overall objective of estimating the probable effectiveness of the proposed surface observational network (PAM II) which will be deployed as part of the winter 1986 GALE field project. This network is to contribute to the study of mesoscale features within developing east coast cyclones, and especially the well-known coastal front.

To accomplish this objective, the process of spatial weighted-averaging interpolation of surface data was investigated by using the Barnes (1973) objective analysis scheme. Tests were conducted to determine the limitations of the Barnes analysis method and evaluate how well this technique reconstructs meteorological fields. A method was developed which enables an optimum weight parameter to be determined for a given data distribution.

Barnes objective analyses were generally more accurate than kinematic fields based on detailed hand analyses. The objective analysis scheme effectively filtered random errors typical of instrumental and exposure effects from the analysis. However, interpolation near the edge of a data domain and extrapolation into data void regions led to

erroneous results.

An optimum weight parameter of 500 $km^2$ was obtained in a mid-west cyclone test case. This resulted in a total response of 0.936 for wavelengths of twice the station spacing.

The Barnes objective analysis method was also used in conjunction with mathematically simulated PAM II data to estimate the probable analysis accuracy of the system (analysis plus network). Analyses based on the present PAM II network design did not adequately represent the true meteorological field containing mesoscale structure. Percentage errors exceeded 100% in the case of temperature advection and local frontogenesis. However, the proposed PAM II network provided analyses nearly as good as those using a twice as dense network, and somewhat better than those obtained using the regular hourly reporting stations.

# APPLICATION OF AN OBJECTIVE ANALYSIS SCHEME TO MESOSCALE OBSERVATIONAL NETWORK DESIGN

by

DEWEY E. HARMS

A thesis submitted to the Graduate Faculty of
North Carolina State University
in partial fulfillment of the
requirements for the Degree of
Masters of Science

Department of
Marine, Earth and Atmospheric Sciences

Raleigh

1 9 8 5

APPROVED BY:

Richard E. Sandlin — David A. Barker

Allen J. Riordan — G. D. Watson
Chairman of Advisory Committee

# BIOGRAPHY

Dewey Elvin Harms was born in Summerdale, Alabama on May 6, 1954. He was reared in the same community and graduated from Foley Senior High School, Foley, Alabama in 1972. In 1975 he received an Associate of Arts degree in Mathematics from Faulkner State Junior College, Bay Minette, Alabama. Two years later he enlisted in the United States Air Force.

He entered North Carolina State University in May of 1979 and received a Bachelor of Science degree with a major in Meteorology in August of 1980. Shortly afterwards, in November, he was commissioned as a second lieutenant in the United States Air Force.

The author held the position of Weather Support Unit Officer at the Eighth Air Force Headquarters, Barksdale Air Force Base, Louisiana. Then, in August of 1983 he entered the Graduate School at North Carolina State University and began studies toward a Master of Science degree in Meteorology.

The author is married to the former Sherilyn Mae Carver and has two sons, Jeremy and Jared. The author's parents, Mr. and Mrs. Ronald Harms, are both living and still reside in Summerdale, Alabama.

# ACKNOWLEDGEMENTS

The author wishes to express his appreciation to the United States Air Force and, in particular, the Air Force Institute of Technology and Air Weather Service for their financial and moral support. He also extends his appreciation to Dr. Gerald Watson, the Chairman of his Advisory Committee, and Dr. David Barber for their aid and advice in the preparation of this thesis. Appreciation is also extended to Dr. Allen Riordan and Dr. Richard Chandler for their helpful suggestions and assistance.

Particular thanks are also given to Raymond Kiess for his aid and consultation concerning computer programmming, and to Rob Blevins and Jim Kroll for their assistance in performing tests necessary for the completion of this study. Finally, the author would like to express his deepest appreciation and gratitude to his wife, Sherilyn, and to his parents and friends for their prayers and continued support, without which this study would not have been possible.

TABLE OF CONTENTS

# CHAPTER 1

## INTRODUCTION

"Objective analysis" is a programmable method for estimating grid point values by transforming (interpolating) data from observations at irregularly spaced points into data at the points of a regular grid mesh. The gridded information can be used for diagnostic studies or in numerical weather prediction models.

The method of analysis is one of the the several factors which determines the analysis accuracy achievable with a given observational network. The accuracy also depends on the observational configuration, density, and frequency; the element being analyzed; and the characteristics of the observational error (Seaman, 1977). This study deals primarily with the method of analysis and with the density and configuration of an observational network to investigate how well the system (analysis plus network) represents true meteorological fields.

This research was conducted in support of the East Coast Project (GALF) to estimate the probable effectiveness of the proposed surface observational network,

the Portable Automated Mesonet (PAM II). Three of the basic objectives of GALE are:

--To observe and document the structure and evolution of mesoscale weather-producing circulation systems associated with mid-Atlantic coastal cyclone development;

--To quantify the physical processes which lead to development of these circulation systems, in particular, coastal frontogenesis;

--To study the relationships between the circulation systems and the significant weather with which they are associated.

The accomplishment of these goals will require the utilization of a mesoscale observing network which describes the circulation systems, that is, resolves the intense gradients which often accompany these systems, and the application of improved diagnostive techniques to the comprehensive data sets which will be collected by this network during GALE.

The purpose of the present research is to investigate the process of spatial weighted-averaging interpolation of surface data using the Barnes (1973) objective analysis scheme. Error analyses are conducted to assess resolution limits of an observing network, in particular, the PAM II observation system.

The combination of the PAM II network with this objective analysis scheme may be considered as a tool for

that forces a high degree of convergence (agreement) between the observed field, $f(x,y)$, and the correction-pass interpolated field, $g_1(x,y)$. Therefore, $k_o$ and $\gamma$ can be used to achieve the desired response of waves in the analysis (Koch et al., 1981, 1983).

With several tests on different data distributions, Barnes (1973) and Koch et al. (1981) have shown that $\gamma$ of approximately 0.3 yields the best results. Specifying $\gamma > 0.4$ does not produce rapid analysis convergence; conversely, using $\gamma < 0.2$ leads to excessive "noise" in the analyzed field. Therefore, a value of 0.3 is used in all tests described in this thesis.

For computational expediency the author modified the weight function $W_n$. The weight is assigned a value of zero if the distance between the grid point and the datum exceeds a chosen critical or "influence" radius $r_c$. The influence radius is assigned a value large enough (6-7 times as large as the average station spacing, $\Delta n$) which insures that only data which would otherwise be weighted extremely small ($W_n < 10^{-80}$) receive zero weight.

The final or "correction-pass" interpolated grid field, $g_1(i,j)$, is the sum of the first pass field and the smoothed residual difference between the observation values, $f(x,y)$, and the first pass estimated values at the data location, $g_o(x,y)$. A simple bilinear interpolation between the values of $g_o(i,j)$ at the four nearest grid

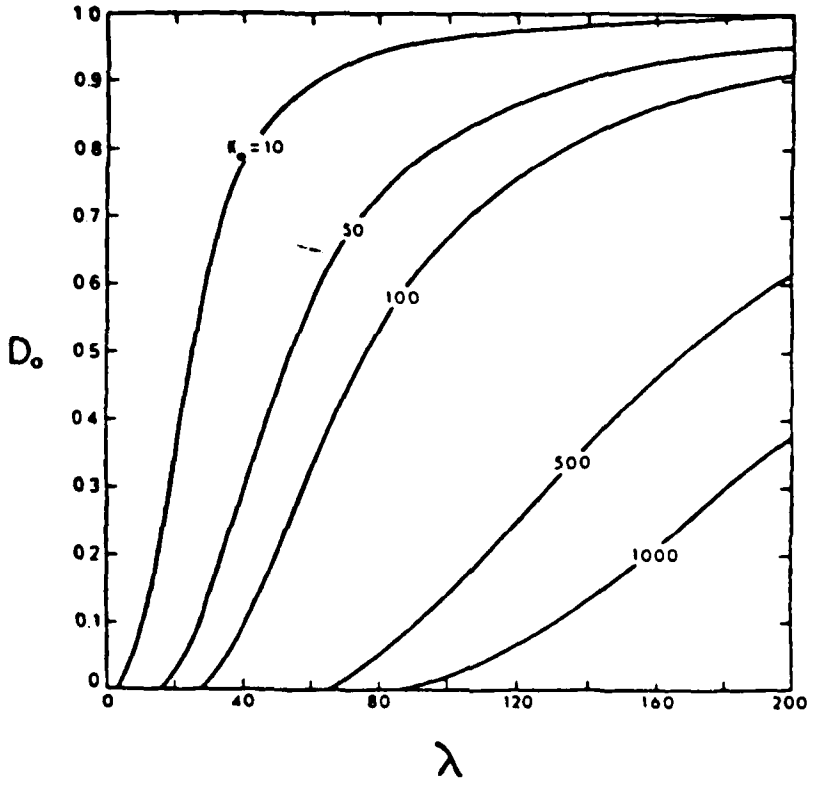


Figure 2.1 - Relationship of first pass response $D_o$ to wavelength $\lambda$ (km) for various values of weight parameter $k_o$ (from Figure 1 of Koch et. al, 1981).

"o" denotes the initial pass.) The interpolated field at grid points is thus given by

$$g_o(i,j) = f(x,y)D_o \ , \qquad (2.3)$$

where f(x,y) is an idealized observed field, that is, a continuum field with no errors. It is important to note that the filter response function that Barnes derived is based upon an idealized field, but in reality only finite sets of observed data with some degree of random error are available. Fig. 2.1 reveals that the incorporation of smaller values of the first pass weight parameter, $k_o$, results in greater filter response, particularly for the short waves.

The original (1964) version of the interpolation scheme required several iterations through the data field. Also, the weight parameter was the same for all passes. Barnes (1973) modified the earlier (1964) version of his technique in order to decrease the computation time necessary to achieve the desired response at small wavelengths. This modification enables a single correction pass through the initial interpolated field to achieve the desired response for specific wavelengths, rather than requiring several iterations as before. This is accomplished by decreasing the weight parameter, k, from its first pass value of $k_o$ to a second (correction) pass value of

$$k_1 = \gamma k_o \ . \qquad (2.4)$$

Here $\gamma$ is a "numerical convergence parameter", $0 < \gamma < 1$,

indicate that the Barnes analysis technique is as good as detailed hand analyses. The inter-comparisons reveal that the differences among the analyses are of the same order as those when the comparison is made with the true data set.

## 2.3 Characteristics of the Barnes Objective Analysis Method

Barnes (1964) developed an objective analysis method that uses a Gaussian weight function in the spatial domain based on the fundamental premise that two-dimensional data distributions can be represented by Fourier integrals. Weights are assigned to the data as a known function of distance between observations and a particular grid point. The weight, $W_n$, is assigned according the distance, $d_n$ (in kilometers, km), between the grid point (i,j) and the datum $f_n(x,y)$ as

$$W_n = \exp(-d_n^2/4k) \ , \qquad (2.1)$$

where k is a weight parameter that determines the shape of the filter response function (the percentage of the original wave's amplitude that will be conserved). (NOTE: k is in units of $km^2$ which will be the assumed units for weight parameters throughout this thesis.)

With one pass through the data, the filter response function can be shown to be

$$D_o = \exp[-k_o(2\pi/\lambda)^2] \ , \qquad (2.2)$$

where $\lambda$ is the the horizontal wavelength. (The subscript

Table 2.1 - Results of a comparison of the Barnes analysis with hand analyses using simulated meteorological fields. Root-mean-square differences among various analyses are presented.

| | Root-Mean-Square Difference | |
|---|---|---|
| | Surface Temperature | 1000 mb Height |
| Barnes / Actual | 0.97 $^{o}$F | 2.38 m |
| Analyst #1 / Actual | 0.79 | 2.67 |
| Analyst #2 / Actual | 0.43 | 3.22 |
| Analyst #1 / Barnes | 0.91 | 3.33 |
| Analyst #2 / Barnes | 1.11 | 3.61 |
| Analyst #1 / Analyst #2 | 0.78 | 2.20 |

pattern scales resolvable by the data distribution will be revealed.

3.) Since the weighting function approaches zero asymptotically, the influence of data may be extended any distance to insure that a sufficient number of observations influence each grid point without changing the weight function and, therefore, the response characteristics.

4.) Only two passes through the data are needed to achieve the desired pattern.

5.) "Noise" is adequately filtered from the analysis so further smoothing by application of additional numerical filters is not necessary.

In support of the choice of the Barnes analysis technique, tests were conducted to compare this analysis method with subjective hand analyses. The hand analyses were performed by two meteorology graduate students with analysis experience. "Bogus" or simulated fields of surface temperature and 1000 mb height were analyzed. (Construction of these fields through utilization of mathematical functions will be discussed at length in Chapter 4.) The resulting grid point values from the two hand analyses and the Barnes scheme were compared to the "true" values at these locations, which were calculated directly with the simulation functions. Inter-comparisons were also made among the three analyses. The results of the comparisons, shown as root-mean-square differences (RMSD) in Table 2.1,

shape of the surface.

Two of the most used successive correction (weighted-averaging) techniques are the Barnes (1973) and Cressman (1959) objective analysis schemes. At first glance, the Cressman scheme may seem more attractive since it does not incorporate a Gaussian weight function and is therefore especially cost effective. However, in this technique, the weight function is dependent on the influence radius beyond which zero weight applies; the weights do not approach zero asymptotically as in the Barnes scheme. To insure that sufficient data influence the interpolation in data sparse regions, the current scan radius is increased locally. This procedure produces unknown response in the final result and introduces short wave features (noise) which must be smoothed by later application of arbitrary filters. Additionally, four or more passes through the data are required in order that Cressman's method achieve the desired pattern.

To summarize, the Barnes (1973) scheme is selected for objective analyses in this study because of the following advantages (listed by Barnes):

1.) The scheme is computationally simple and assigns weights solely as a function of distance between datum and grid point.

2.) The weight parameter, which determines the degree of smoothing, can be chosen prior to the analysis so that

in this study because of its simplicity, accuracy, cost effectiveness, and its several advantages (mentioned later) over similiar techniques. The method of statistical interpolation was not chosen since this technique is complex, and also tends to exhaust computer resources when calculating the observational and initial guess correlations which determine the weighted coefficients. Furthermore, Otto-Bliesner et al. (1977) showed that this method is no better or worse than methods similar to the Barnes scheme (successive corrections) when the analyses are performed over a data-rich region. The variational technique of Sasaki (1958, 1970) also attempts to accomplish not only the interpolation phase of objective analysis but also the matching of variables (data assimilation) which requires additional computation time. For the purposes of this research, only the interpolation of observational data to a regular grid is necessary.

In the past the method of polynomial (surface) fitting has been successful in accomplishing the desired interpolation. However, according to Barnes (1964), such schemes possess three major disadvantages: the calculations are complicated and costly with respect to computer time; the data to which the surface is fitted are chosen in a rather artificial manner (that which produces the best results); and the effect of erroneous data can be disastrous since each datum is given equal ranking in determining the

minimum; also, they depend upon the spatial covariances among the analyzed variables. Examples of this technique are found in Gandin (1963), Eddy (1967), Bengtsson and Gustavsson (1971), Rutherford (1972, 1973), Thiebaux (1975), and Schlatter et al. (1976).

3.) Variational Technique. The method, developed by Sasaki (1958, 1970), is a post-analysis adjustment technique based upon the calculus of variations. A functional is utilized which minimizes the analyzed-minus-observed differences, filters undesirable high-frequency and high-wave number features, and employs dynamical constraints. These constraints may be strong (satisfied exactly) or weak (satisfied only approximately). This method is effective in making the analyzed fields compatible with a forecast model.

4.) Polynomial Fitting. Observations are fitted by utilizing polynomials of two or more variables. The fit is obtained by a least squares technique since there are often fewer polynomial coefficients than data points. Polynomial fitting techniques have been used by Panofsky (1949), Gilchrist and Cressman (1954), Penn et al. (1963), and Shapiro and Hastings (1973).

## 2.2 Comparison of the Barnes and Alternative Schemes

The Barnes objective analysis scheme was chosen for use

To review the different methods of objective analysis, four of the more prominent techniques are summarized (Schlatter et al., 1976):

1.) Successive Corrections. A forecast model or an interpolation from first pass-grid values back to station locations provides the preliminary estimate (first-guess) of the field to be analyzed. This estimate is modified by a combination of corrections computed for each grid point. The corrections are proportional to the differences between the observed and first-guess values. These are weighted empirically, with observations nearest the grid point weighted most heavily. Several scans or passes are made through the data; the results of one scan become the first guess for the next scan. Bergthórsson and Döös (1955), Cressman (1959), and Barnes (1964, 1973) have developed analysis schemes based upon the successive corrections method.

2.) Statistical (Optimum) Interpolation. This analysis technique, based on statistical linear regression, incorporates either a forecast model, persistence, or climatology as a first-guess field. The analyzed value at a grid point is the sum of this first-guess and a linear combination of corrections, which are proportional to the differences between observational and first-guess values. The weighting coefficients are determined from the condition that the mean-square-error of the analyzed values be a

smoothing is essential to producing fields that will provide meaningful estimates of such derived quantities as divergence, advections, and gradients from the grid point values (Koch et al., 1981).

As noted by Gandin (1963), the term "objective analysis" is, to some extent, misleading. The analysis of a meteorological field does not imply the reconstruction of the whole field. Actually it implies a study of the properties of an already constructed field. Thus, according to Gandin, "numerical methods for the reconstruction of meteorological fields" would be a more appropriate term. However, the term "objective analysis" will be used in this text since it is widely accepted and used.

Objective analysis performs three basic tasks: 1.) the interpolation of values of observed meteorological elements to grid points, 2.) the assimilation of raw data, a process in which meteorological observations are absorbed into a numerical representation of the atmosphere, and 3.) the detection and elimination of erroneous data. "Assimilation may be distinguished from interpolation by requiring that the numerical representation be a complete description of meteorological variables whose mutual dependence is governed by explicit physical constraints" (McPherson, 1975). Of the three basic tasks listed, the first (interpolation) is the most important part of objective analysis and will be investigated at length in this paper.

# CHAPTER 2

# BARNES OBJECTIVE ANALYSIS METHOD

Before an in-depth description of the Barnes objective analysis method is presented, it is appropriate to first review the purpose and content of objective analysis, and to provide a brief summary of the better known methods.

## 2.1 Review of Objective Analysis Methods

Objective analysis involves the development of mathematical methods which use data at irregularly spaced points to reconstruct objectively the continuous field of some meteorological variable, and to display this field at a regular set of grid points. The data in this format then permit quantitative diagnostic and/or predictive calculations to be made.

The process of objective analysis results in the smoothing (suppressing) of, especially, the higher frequency, shorter wavelength features, including unavoidable "noise", and those arising from large data errors or nonrepresentative observations. Controlled

through the utilization of simulated meteorological fields, the influence of this analysis technique on the reconstructed fields. In addition, an estimate is made of the confidence with which kinematic fields can be evaluated by superposing random errors typical of instrumental and site exposure variability on the simulated field. This procedure, to some extent, evaluates the limitation of a meteorological network in measuring or describing mesoscale weather systems. Furthermore, these tests can be helpful in making final adjustments to the proposed PAM II network design, and possibly in developing strategies for the deployment of mobile observing systems for the GALE project.

obtaining estimates of meteorologically significant parameters such as vorticity, divergence, gradients, and advections. To obtain an estimate of how well that tool will function, the Barnes objective analysis scheme is applied to bogus data sets which include a reasonable error component. These data sets are developed by judicious enhancement of case study results using a simulation model of known mathematical form, and dependent only on a station's location. Using existing studies of coastal fronts, gradients are sharpened beyond those which can be resolved by the observation network while not violating any of the data. Values (from the resulting fields) which correspond to the proposed PAM II station locations are used as simulated observational data. These "observations" based on the known field are then made more realistic by adding a reasonable error component. Finally, these data are analyzed to a mesoscale grid. The resulting derived fields are compared with those obtained without the introduction of error and to the "true" simulated field values at the corresponding grid points.

More specifically, the task of this research effort is to utilize a highly flexible version of the Barnes objective analysis scheme to perform tests to determine optimum weight parameters (which control the degree of smoothing performed in the analysis) to be used in the study of mesoscale processes. An attempt is also made to isolate and study,

points is used to estimate $g_o(x,y)$. The final field is given by

$$g_1(i,j) = g_o(i,j)+[f(x,y)-g_o(x,y)]D_1 \quad . \tag{2.5}$$

Here

$$\begin{aligned} D_1 &= \exp[-k_1(2\pi/\lambda)^2] \\ &= \exp[-\gamma k_o(2\pi/\lambda)^2] = D_o^{\gamma} \end{aligned} \tag{2.6}$$

is the response function corresponding to the weight function

$$\begin{aligned} W_n' &= \exp(-d_n^2/4\gamma k_o) \quad , \; d_n \leq r_c \\ &= \quad 0 \quad\quad\quad , \; d_n > r_c \quad . \end{aligned} \tag{2.7}$$

The actual correction-pass value at each grid point results from adding the weighted averages from the two passes with N observations (This follows from 2.5.):

$$g_1(i,j) = \frac{\sum_{n=1}^{N} W_n f_n(x,y)}{\sum_{n=1}^{N} W_n} + \frac{\sum_{n=1}^{N} W_n'[f_n(x,y)-g_o(x,y)]}{\sum_{n=1}^{N} W_n'} \tag{2.8}$$

Substituting (2.6) and (2.3) into (2.5) gives

$$\begin{aligned} g_1(i,j) &= D_o f(x,y)+[f(x,y)-D_o f(x,y)]D_o^{\gamma} \\ &= f(x,y)D_o(1+D_o^{\gamma-1}-D_o^{\gamma}) \; ; \end{aligned} \tag{2.9}$$

therefore, the true correction pass (total) response function is

$$D_T = D_o(1+D_o^{\gamma-1}-D_o^{\gamma}) \quad . \tag{2.10}$$

This total response function, $D_T$, indicates the degree of analysis convergence, that is, how closely the

interpolated values agree with the observed ones. Fig. 2.2 shows that the second pass through the data will increase the degree of convergence when $0 < \gamma < 1$.

Koch et al. (1981) have proven that the 1973 version of the Barnes objective analysis technique is absolutely convergent. This fact enables the analyst to control the amount of small-scale detail to be revealed in the analyzed data fields.

## 2.4 Computer Program Package

The author has developed a computer program which instills versatility in the objective analysis through human selection of input parameter values: grid spacing and origin, weight parameter, and numerical convergence parameter. Before the analysis computations are performed, a rectangular coordinate system with an array of grid points is constructed using a polar stereographic map projection (Inman, 1970). The grid can be constructed over any area of the earth at any desired orientation. A highly flexible input routine allows easy manipulation of raw data. The objective analysis procedure follows the logic outlined in Section 2.3.

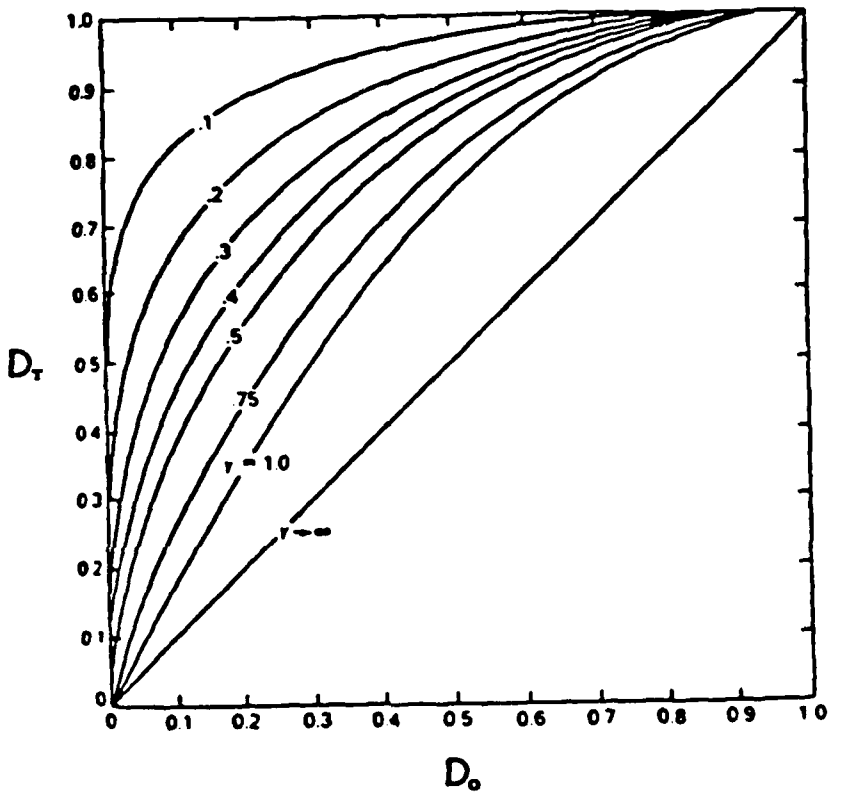


Figure 2.2 - Total response function $D_T$ after the correction pass as a function of initial response $D_o$ and numerical convergence parameter $\gamma$ (from Figure 3 of Barnes, 1973).

## 2.5 Research Goals

Through the use of the Barnes objective analysis scheme, several goals of this research are achieved. The goals include:

1.) Determination of "edge" effects; that is, how the analysis scheme behaves near the edge of, or beyond the data domain.

2.) Determination of the optimum weight parameter and grid spacing for a given data distribution.

3.) Determination of the effects of incorporating random error in a data field.

4.) Determination of the Barnes scheme's effects on the character of the information it processes.

5.) Obtaining an a priori estimate of typical errors which may occur in the basis and derived kinematic fields based on GALE PAM II data.

6.) Determination of whether the proposed PAM II network produces analyses significantly better than those obtained from the regular hourly reporting station network.

7.) Experimentation with alternative PAM II networks to test their impact on the depiction of features of particular interest to GALE project goals.

The following chapter describes a test case in which the first three objectives are investigated.

# CHAPTER 3

# EXPERIMENTS WITH THE BARNES ANALYSIS METHOD ON A MID-WEST CYCLONE

## 3.1 Overview and Synoptic Situation

The case of 9 November 1983 (2100 GMT) over the central United States was used to test the Barnes objective analysis computer program, and to investigate "edge" effects, optimum weight parameter, effects of random error on data fields, and overall accuracy as compared to subjective analyses. The mid-west test case provided non-uniform fields and strong gradients needed to test the limitations of the Barnes objective analysis and determine how well this technique reproduces true meteorological fields.

This particular case features a mature surface cyclone with a sharply-defined frontal system over the Central Plains (Fig. 3.1). To be noted are the pronounced temperature gradient and cyclonic shear through the frontal zone and the strong pressure gradient west of the cyclone with a rather weak gradient to the east. Since precipitation was occurring at the chosen synoptic time

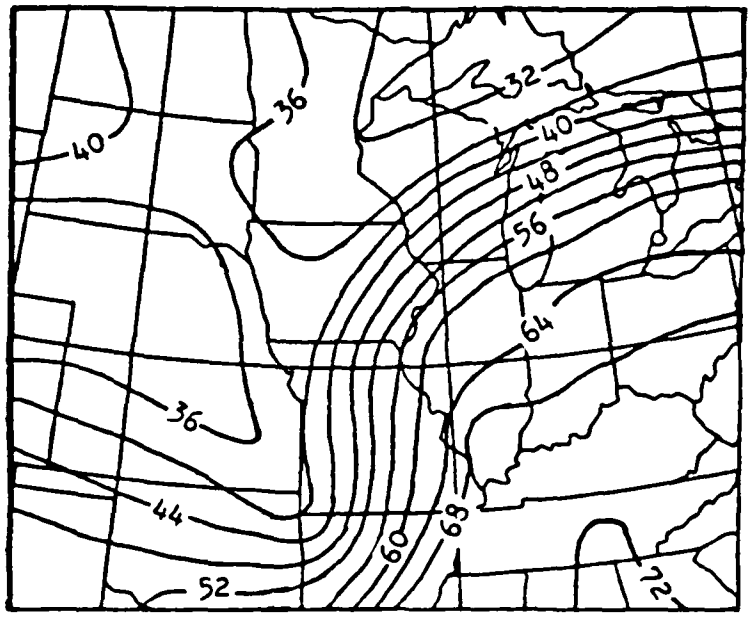


Figure 3.1a - Hand analysis of surface temperature ($^{o}$F) for 2100 GMT 9 November 1983. Contours are drawn with interval of 4 $^{o}$F.

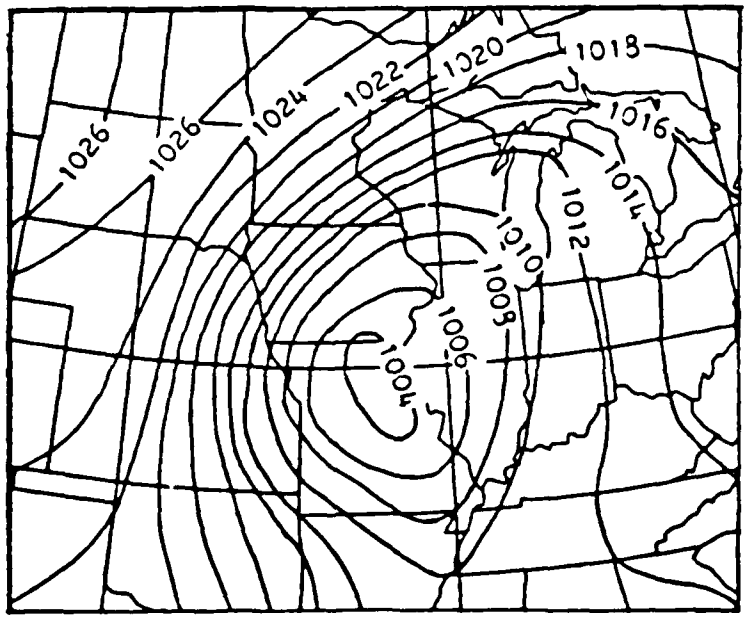


Figure 3.1b - Hand analysis of sea level pressure (mb) for 2100 GMT 9 November 1983.

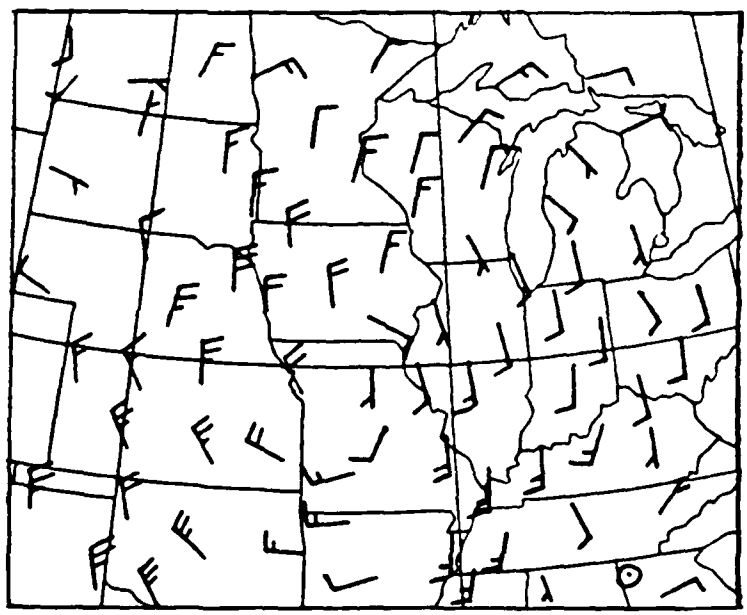

Figure 3.1c - Hand plot of a representative sample of the wind reports for 2100 GMT 9 November 1983. Wind barbs are plotted using standard notation with speed in knots.

(2100 GMT), a qualitative comparison of these areas can be made with the objectively analyzed patterns of surface convergence and relative vorticity.

The objective analysis was performed over a rectangular area whose sides extend from North Dakota to the Texas Panhandle to northern Georgia to the upper Great Lakes region. A total of 143 station observations were incorporated into the analysis. A 15X18 grid was constructed on a regular coordinate system with the x- axis along the central longitude of the grid positive to the south and the y- axis positive to the east at the center of the grid. A grid spacing of 115 km was used. An inner grid encompassing the central 35 stations of the total network was also used in various tests.

A qualitative comparison of Barnes and hand analyses of pressure and temperature patterns can be made by examining Figs. 3.1 and 3.2. Fig. 3.2c shows the wind field based on an analysis of the wind components. (The u- and v- components of the observed winds were analyzed seperately; then these objectively analyzed grid values of u- and v- were added to obtain wind speeds and directions at the grid points.) The objectively analyzed wind field may be compared with the plotted winds in Fig. 3.1c.

Fig. 3.3a shows the precipitation reports superimposed on the surface divergence pattern produced from the Barnes analyzed u- and v- wind components. The precipitation

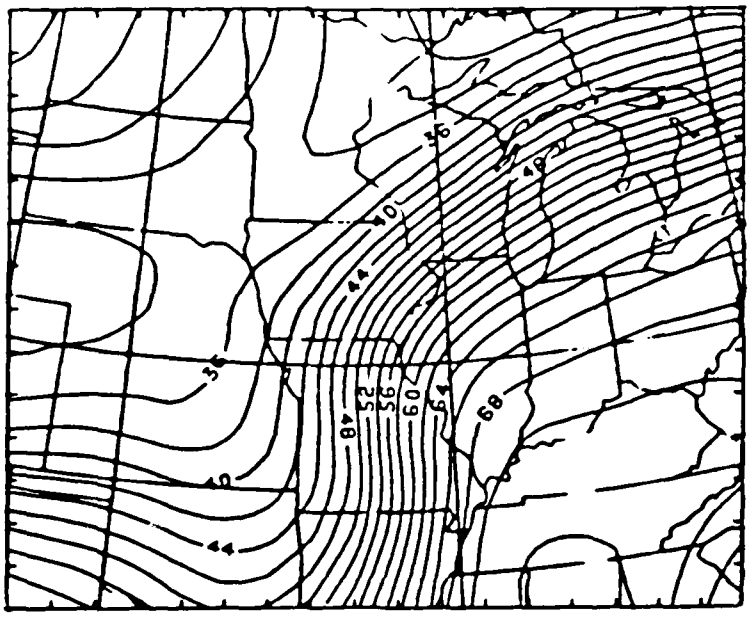


Figure 3.2a - Barnes analysis of surface temperature ($^{o}$F) for 2100 GMT 9 November 1983 ($k_o$ = 500).

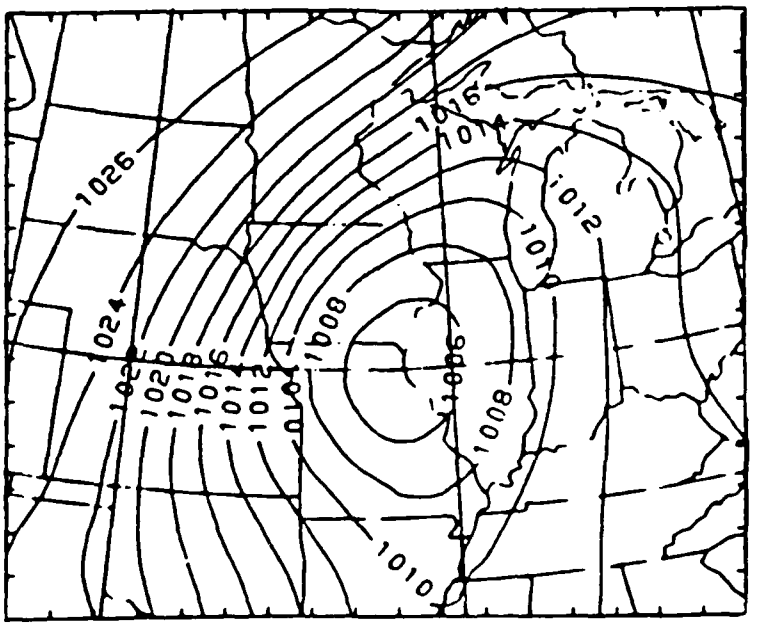


Figure 3.2b - Barnes analysis of sea level pressure (mb) for 2100 GMT 9 November 1983 ($k_o$ = 500).

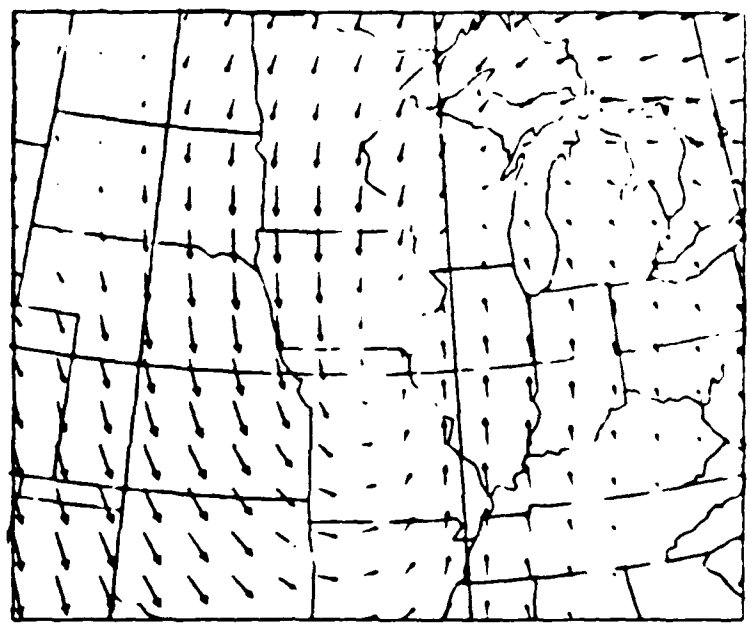

Figure 3.2c - Vector display of Barnes analysis of surface winds for 2100 GMT 9 November 1983 ($k_o$ = 500).

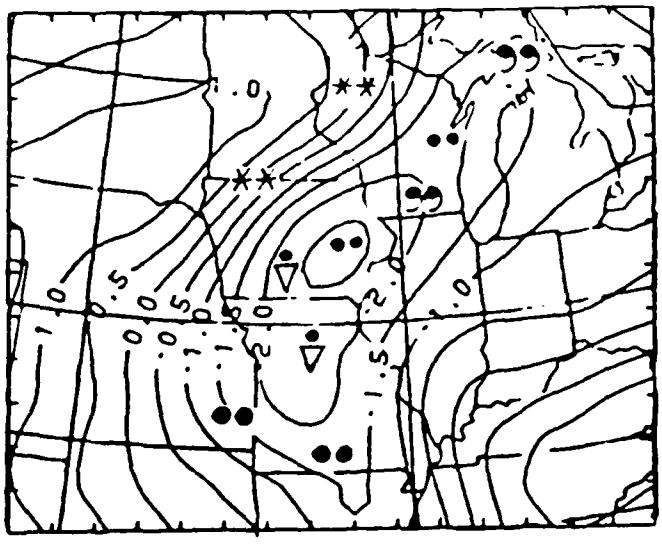

Figure 3.3a - Surface divergence ($10^{-5}$/s) derived from Barnes analyzed wind components for 2100 GMT 9 November 1983. Precipitation reports are superimposed.

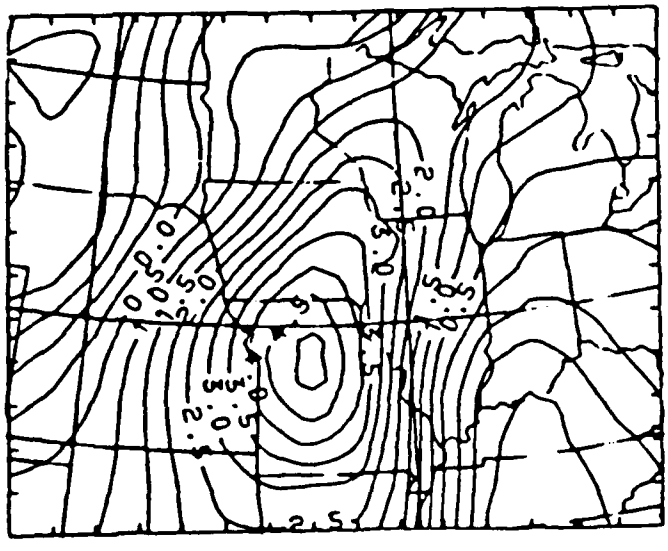

Figure 3.3b - Vertical component of relative vorticity ($10^{-5}$/s) derived from Barnes analyzed wind components for 2100 GMT 9 November 1983.

pattern approximately coincides with the axis of maximum convergence. The objective analysis of surface relative vorticity (Fig. 3.3b) shows maximum positive vorticity along the trough and at the low pressure center, as one would expect.

In each of the above figures the graphic package (SURFACE II), developed at the University of Kansas, was used to objectively contour the gridded data (Figs. 3.2 and 3.3). Thus, the analyses are produced with complete objectivity by the computer.

## 3.2 Edge-Effect Test

It would be advantageous to an analyst to know how the analysis scheme behaves near the edge of the data field. With this information one can decide whether to retain or reject the gridded values near the edge of or beyond the data domain. If these values are accepted, one will have a better insight into their reliability. The following steps were taken to help determine these effects:

1.) The Barnes analysis was performed over the entire grid using all 143 stations. This analysis was used to provide standard or "true" values over the entire region.

2.) The objective analysis was then performed over an inner array (centered within the larger grid) of 11X11 grid points and using 35 stations. An inner-most 7X7 grid array

approximately coincided with the region encompassing these stations.

3.) Each of the grid point values from the smaller grid was subtracted from the corresponding grid value in the larger grid. Root-mean-square errors (RMSE) were calculated using the values of the peripheral grid points of each successive smaller square of grid points, where N = 40, 32, 24, 16, and 8 for the successive squares, using:

$$RMSE = \{[\sum_{1}^{N} (GP_L - GP_S)^2]/N\}^{0.5} \qquad (3.1)$$

where $GP_L$ is the grid point value from the 15X18 grid and $GP_S$ is the corresponding value from the inner grid.

The results, shown in Table 3.1, reveal a significant increase in error near the edge of the data field with approximately a 200-300% increase in error from the edge of the data domain (7X7) to the outer square (11X11). Hence, it is shown that extrapolation into data void regions leads to extremely erroneous results and even as the edge of the data domain is approached the interpolation becomes unreliable.

## 3.3 Weight Parameter and Random Error Tests

The choice of a weight parameter for a given data distribution is critical since the weight determines the

Table 3.1 - "Edge Effects Test": Root-mean-square-error for successive peripheral squares of grid points for which the 15X18 grid serves as the standard. Total number of grid points is given for each square. Results for temperature and wind components are shown.

| | 11X11 sq. (40 pts.) | 9X9 (32) | 7X7 (24) | 5X5 (16) | 3X3 (8) |
|---|---|---|---|---|---|
| TEMP ($^{o}$F) | 2.80 | 1.59 | 1.06 | 0.89 | 0.63 |
| U (m/s) | 3.71 | 2.22 | 1.10 | 0.48 | 0.26 |
| V (m/s) | 1.03 | 0.93 | 0.76 | 0.52 | 0.30 |

# CHAPTER 4

# A SIMULATION OF METEOROLOGICAL FIELDS

## 4.1 Construction of the Analytic Functions

To determine how well a particular arrangement of the PAM II network will provide estimates of meteorologically significant parameters such as divergence, vorticity, temperature gradient and advection, experimental "bogus" data sets will be used with the Barnes objective analysis. Meaningful tests of this analysis method require data sets at both grid and observation points. A simulation model incorporating mathematical functions which are dependent on a point's latitude and longitude is chosen to generate meteorological fields of temperature and geopotential height. These analytical fields should resemble actual meteorological fields and possess enough non-linearity to identify problems and merits of the observing network and interpolation scheme being tested.

The analytic functions chosen are based upon Sanders' (1971) structural model of temperature and height fields which he used to find analytic solutions to the

Table 3.6 - Effects on optimum weight parameter and RMSEs due to increasing the grid spacing. (Same as Table 3.5b except DX = 115 km.)

(Divergence and vorticity in units of $10^{-5}$/s, wind components in units of m/s)

| | Root-Mean-Square-Error | | | |
|---|---|---|---|---|
| $k_o$ | DIV | VORT | U | V |
| 12.5 | 0.93 | 0.85 | 1.44 | 1.20 |
| 25. | 0.83 | 0.62 | 1.01 | 0.99 |
| 50. | 0.80 | 0.61 | 0.85 | 0.76 |
| 100. | 0.80 | 0.85 | 0.98 | 0.50 |
| 250. | 1.09 | 1.19 | 1.22 | 0.54 |
| 500. | 1.51 | 1.41 | 1.70 | 0.76 |
| 1000. | 1.91 | 1.80 | 2.34 | 0.92 |
| 1500. | 2.16 | 2.09 | 2.75 | 0.99 |
| 2000. | 2.22 | 2.30 | 3.03 | 1.03 |
| 3000. | 2.35 | 2.54 | 3.39 | 1.08 |
| 5000. | 2.47 | 2.75 | 3.73 | 1.13 |

(DX = 115 km) twice as large as before to determine if there is a significant difference in the mean errors and the optimum weight parameter of the kinematic fields when DX is varied. When the results of Table 3.6 (DX = 115 km) are compared to those of Table 3.5b (DX = 57 km), it is readily apparent that the optimum weight of each of the four variables remained the same except in the case of vorticity, where the optimum weight parameter decreased slightly. The minimum error did not increase a significant amount with the coarser grid; in fact, the error in vorticity actually decreased somewhat. These results concur with the findings of the test in Section 3.3.1 which incorporated the "missing station" procedure. Therefore, it is concluded that using a grid spacing significantly smaller than the average station spacing ($DX < \Delta n/2$) is not justified when computing costs are considered.

The results from the more reliable test method (more reliable since the standard was the actual known station value) in Section 3.1.1 showed the optimum weight parameters for the u- and v- wind components to be approximately 250 and 500, respectively (Table 3.2). This suggests that the optimum weight parameters determined using hand analyses as the standard may be biased toward too small values. Therefore, if the optimum weight for divergence and vorticity is again taken to be twice as large as that for u- and approximately equal to that of v-, the appropriate optimum $k_o$ for the kinematic variables would be approximately 500 for the given station distribution.

With an average station spacing of approximately 95 km and $k_o$ of 500, the total response (Equation 2.10) of the 2 $\Delta n$ wave is found to be 0.936. With this total response an "optimum" weight parameter can be calculated (using Equations 2.2 and 2.10) for similar data distributions with known average station spacings.

The calculated response of 0.936 may seem rather high, especially compared to Koch's (1981) suggestion that this response should equal 1/e or 0.3679. However, to achieve a total response of 1/e for 2 $\Delta n$ waves and $\gamma = 0.3$, $k_o$ would have to be approximately 3200. From the results in Fig. 3.4 it is apparent that the error would be unacceptably large, primarily due to over-smoothing.

This test was repeated using a grid spacing

shows the RMS differences of each individual analysis compared to the average of the other four analyses. The average of all five subjective analyses served as the standard for comparison with the objectively analyzed variables.

The observed u- and v- wind component fields were objectively analyzed using various weight parameters. These analyzed fields were then used to compute divergence and vorticity fields. Table 3.5b shows the error for each variable at all $k_o$'s tested. The RMSE of the optimum weight for each variable was almost as low as the error of the best hand analysis of the corresponding variable, particularly for divergence and vorticity. For these derived fields the minimum RMSE was less than the majority of the hand analysis results. Unfortunately, the error in the divergence and vorticity approaches the same order of magnitude as the values themselves.

The results in Table 3.5b enable some conclusion to be drawn on the choice of an optimum weight parameter. The optimum $k_o$ for divergence and vorticity is about 100 and is approximately equal to that for v- and approximately twice that for the u- wind component (optimum $k_o$ = 50). This suggests that the original fields (temperature, wind components, etc.) may require smoother analyses when kinematic fields (finite-differenced values) are to be constructed.

Table 3.5a - Root-mean-square differences of each hand analysis compared to the average of the other four analyses with DX = 57 km. Results for surface divergence, relative vorticity, and wind components are shown.

(Divergence and vorticity in units of $10^{-5}$/s , wind components in units of m/s)

| | DIV | VORT | U | V |
|---|---|---|---|---|
| Analyst #1 | 1.44 | 1.02 | 0.86 | 0.96 |
| Analyst #2 | 0.98 | 0.79 | 0.60 | 0.47 |
| Analyst #3 | 1.10 | 0.78 | 0.73 | 0.30 |
| Analyst #4 | 0.76 | 0.80 | 0.76 | 0.38 |
| Analyst #5 | 1.48 | 1.11 | 0.75 | 1.16 |

---

Table 3.5b - Weight parameter test using kinematic variables with DX = 57 km. Root-mean-square-errors for each weight parameter are presented for which the average of the five hand analyses served as the standard.

| $k_o$ | DIV | VORT | U | V |
|---|---|---|---|---|
| 12.5 | 1.99 | 2.07 | 1.31 | 0.91 |
| 25. | 1.49 | 1.59 | 0.90 | 0.90 |
| 50. | 1.03 | 1.10 | 0.79 | 0.73 |
| 100. | 0.77 | 0.78 | 0.97 | 0.48 |
| 250. | 1.03 | 1.14 | 1.23 | 0.54 |
| 500. | 1.47 | 1.39 | 1.71 | 0.76 |
| 1000. | 1.91 | 1.81 | 2.34 | 0.92 |
| 1500. | 2.12 | 2.13 | 2.75 | 0.99 |
| 2000. | 2.25 | 2.35 | 3.03 | 1.03 |
| 3000. | 2.39 | 2.62 | 3.38 | 1.07 |
| 5000. | 2.52 | 2.86 | 3.73 | 1.12 |

The comparison of Table 3.4 (with error) and Table 3.3 (without error) reveals the optimum weight parameter for each variable remains unchanged. Unexpectedly, the RMSE corresponding to the optimum $k_o$ decreases slightly when random errors are added to the temperature and v- fields. However, with several of the non-optimum $k_o$'s the error increases, as would be expected. In any event, the results for all the variables indicate that the Barnes objective analysis effectively eliminates the effects of random errors.

### 3.3.3 Tests employing kinematic variables

A weight parameter should be chosen which minimizes the error in the kinematic fields such as temperature advection, divergence, vorticity, and horizontal moisture convergence since these are especially meteorologically significant; that is, they are directly related to the genesis and maintenance of weather systems. Therefore, a test to determine the optimum weight parameter for these computed quantities is presented here.

Analyses of the u- and v- wind components performed by five NCSU faculty and graduate students served to produce a standard against which to compare the Barnes analysis results. Divergence and vorticity values were calculated using these analyses of the wind components. Table 3.5a

Table 3.3 - Results from optimum weight parameter test with DX = 115 km.

| | Root-Mean-Square-Error | | |
|---|---|---|---|
| Weight Parameter | Temperature | U- component | V- component |
| 12.5 | 2.86 °F | 3.69 m/s | 3.12 m/s |
| 25. | 2.82 | 3.55 | 3.04 |
| 50. | 2.79 | 3.39 | 2.90 |
| 100. | 2.66 | 3.16 | 2.70 |
| 250. | 2.89 | 3.15 | 2.50 |
| 500. | 3.67 | 3.47 | 2.42 |
| 1000. | 4.97 | 3.96 | 2.41 |
| 1500. | 5.86 | 4.33 | 2.44 |
| 2000. | 6.49 | 4.68 | 2.47 |
| 3000. | 7.27 | 4.97 | 2.52 |
| 5000. | 8.04 | 5.34 | 2.57 |

---

Table 3.4 - Same as Table 3.3 except random errors have been incorporated into the observation data, with standard deviation of random error of 2 °F and 2 m/s for the surface temperature and wind components, respectively.

| | Root-Mean-Square-Error | | |
|---|---|---|---|
| Weight Parameter | Temperature | U- component | V- component |
| 12.5 | 3.05 °F | 3.61 m/s | 3.25 m/s |
| 25. | 2.82 | 3.48 | 3.06 |
| 50. | 2.72 | 3.32 | 2.76 |
| 100. | 2.51 | 3.18 | 2.45 |
| 250. | 2.62 | 3.23 | 2.20 |
| 500. | 3.40 | 3.56 | 2.19 |
| 1000. | 4.75 | 4.04 | 2.26 |
| 1500. | 5.70 | 4.42 | 2.32 |
| 2000. | 6.36 | 4.66 | 2.37 |
| 3000. | 7.19 | 5.01 | 2.44 |
| 5000. | 8.09 | 5.36 | 2.57 |

much less than the u- components.

The same test was repeated but with the grid spacing doubled. The purpose was to determine the effect on the optimum weight parameter and the least RMSE when the interval between grid points is changed. The results in Table 3.3 show that the optimum $k_o$ for each variable remains the same. Also worth noting, the minimum error is only slightly less when using the denser grid; at the same time, the computation required is four times greater, which probably does not justify using a grid spacing much less than the station spacing, in this case, approximately 95-100 km.

### 3.3.2 Tests on data fields with random error

To substantiate the above findings on optimum weight parameters, a similar test is conducted with additional random error added to the fields. The random errors are generated by a computer and have a Gaussian distribution with a mean of zero and standard deviation of 2 $^{o}$F for temperature and 2 m/s for the wind components. This procedure should reveal the weight parameter which yields the optimum smoothing of random error, that is, the most effective high frequency noise filter. The actual station values without the random errors are again used as the standard.

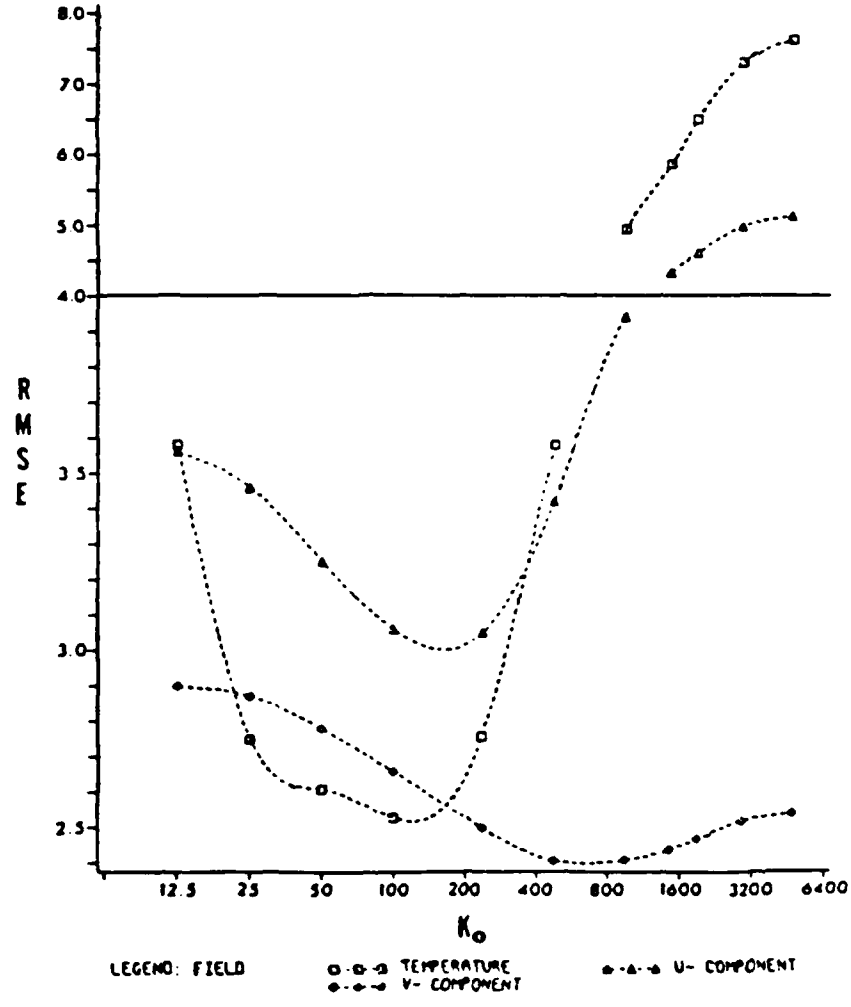


Figure 3.4 - Graph of root-mean-square-error (RMSE) for various weight parameters ($k_o$) with DX = 57 km. RMSEs are in units of $^{o}$F for temperature and m/s for wind components. (NOTE: on the RMSE axis the linear scale changes at 4.0)

Table 3.2 - Results from optimum weight parameter test with DX = 57 km. Root-mean-square-error for various weight parameters are shown.

| | Root-Mean-Square-Error | | |
|---|---|---|---|
| Weight Parameter | Temperature | U- component | V- component |
| 12.5 | 3.58 $^{o}$F | 3.56 m/s | 2.90 m/s |
| 25. | 2.75 | 3.46 | 2.87 |
| 50. | 2.61 | 3.25 | 2.78 |
| 100. | 2.53 | 3.06 | 2.66 |
| 250. | 2.76 | 3.05 | 2.50 |
| 500. | 3.58 | 3.42 | 2.41 |
| 1000. | 4.93 | 3.94 | 2.41 |
| 1500. | 5.85 | 4.32 | 2.44 |
| 2000. | 6.48 | 4.60 | 2.47 |
| 3000. | 7.27 | 4.96 | 2.52 |
| 5000. | 7.58 | 5.11 | 2.54 |

for this station.

3.) Steps 1.) and 2.) are repeated for each of a succession of missing stations chosen at random from the total station population.

4.) Then an RMSE is calculated by computing the difference of the observed and the interpolated values at the missing station for each analysis.

5.) Steps 1.) through 4.) are then repeated for each of the remaining $k_o$'s to be tested.

As shown in Table 3.2 an optimum weight with a minimum error is obtained for each variable. Fig. 3.4 shows the graph of these results; rather well-defined minima of error are depicted in the case of temperature and u- component of the wind. For temperature a $k_o$ of approximately 100 produced the minimum error, while $k_o$ lay between 100 and 250 for u- and between 500 and 600 for the v- component of the wind. These results suggest that a weight parameter of approximately 250 would be optimal for the meteorological variables considered in this particular case. This type of compromise would result in a slight "over-smoothing" of the temperature field and "under-smoothing" (noise) of the v-component wind pattern. The apparent discrepancy of the smaller v- field RMSEs as compared to those of the u- field is, in part, due to the fact that the v- components (generally, the east-west components since the y- axis of the coordinate system is defined positive to the east) were

Barnes analysis is performed over the field except that a single station observation left out. Then bilinear interpolation of the four surrounding grid values from the Barnes analysis is used to obtain an estimate at the missing station location. RMSEs are calculated using the station's actual observed value as the standard. This method gives a realistic measure of error since the datum at the point of interpolation is not in the data set utilized by the analysis scheme. However, if this datum was incorporated and then an interpolation made back to the point, the error could approach zero as $k_o$ approaches zero since locally that single datum almost exclusively influences the surrounding grid point values. On the other hand, one might expect that if $k_o$ becomes too small in a "missing station" test short-wavelength noise will increase the error; and if $k_o$ becomes too large excessive smoothing will occur and the error again increases. Therefore, one can reasonably expect an optimum $k_o$ with some minimum RMSE.

The test is conducted in the following manner:

1.) Using a 15X15 grid (grid spacing, DX of 57 km; one-half of that used in the "edge-effect" test) encompassing the inner 35 stations and a given $k_o$, the objective analysis is performed with one station missing.

2.) Through bilinear interpolation of the four surrounding grid values, an estimated value is calculated

response of the features in the analysis, that is, the percentage of the amplitude of each wavelength that is retained. The weight parameter is dependent on wavelength and can be specified for the smallest resolvable wave (twice the station spacing = 2 $\Delta n$) when the response for the resolvable scale is prescribed. Barnes (1973) did not offer clear guidance for the selection of $k_o$ in the spatial weight function. His choice for this parameter was rather arbitrary by suggesting that one should know beforehand what the response of the smallest resolvable scale should be as a function of the accuracy or representativeness of the data.

Koch et al. (1981) suggested guidelines for choosing the weight parameter. It was suggested that the parameter be selected such that a maximum response of 1/e (.3679) at the 2 $\Delta n$ scale is achieved. However, in the present author's opinion, the choice of 1/e as the maximum response for the smallest resolvable wave is also arbitrary. Koch did not present the reasoning behind his choice. Therefore, several tests were made to determine an optimum weight parameter for a given data distribution; that is, one that yields the least error in the analyzed field.

### 3.3.1 Optimum weight parameter tests

The approach taken to determine an optimum weight parameter ($k_o$) is the "missing station" method. The

nonlinear quasi-geostrophic omega and vorticity equations. Koelher (1979) also used Sanders' model with certain modifications in order to provide a better large-scale representation of meteorological fields. A number of modifications are employed here to enhance temperature gradients and to sharpen and re-orient height (pressure) troughs.

Sanders defined the 1000 mb height field as a function of x and y (horizontal distance parameters), and the temperature as a function of x, y, and pressure. His expressions for these fields are given in Equations 4.1 and 4.2, where x and y in his original functions have been replaced by their latitudinal and longitudinal equivalents.

$$Z(\lambda,\phi,1000) = \bar{Z} \cos[(\lambda_o-\lambda+\Delta\lambda)2\pi/L_\lambda] \cos[(\phi-\phi_o)2\pi/L_\phi)] \quad (4.1)$$

$$T(\lambda,\phi,p) = {}_m(p) - [1-\beta\ln(1000/p)] \{\eta r(\phi-\phi_o) + \bar{T} \cos[(\lambda_o-\lambda)2\pi/L_\lambda] \cos[(\phi-\phi_o)2\pi/L_\phi]\} \quad (4.2)$$

where $\lambda$ = longitude in radians

$\phi$ = latitude in radians

p = pressure in millibars

$L_\lambda$ = east-west wavelength in radians of longitude

$L_\phi$ = north-south wavelength in radians of latitude

$\lambda_o$ = reference longitude

$\phi_o$ = reference latitude

$\Delta\lambda$ = a parameter which controls the phase lag of the 1000 mb height field relative to the temperature field in radians of longitude

$T_m(p)$ = mean temperature at pressure p

$\bar{Z}$ = amplitude of the 1000 mb height disturbance

$\bar{T}$ = amplitude of the 1000 mb temperature field

$\beta$ = a parameter that determines the pressure at which the reversal of temperature gradient appears

r = radius of the earth

$\eta$ = magnitude of the mean north-south temperature gradient.

Since the purpose here is to develop a two-dimensional model of meteorological fields at or near the surface of the earth, the temperature expression can be simplified by letting p = 1000, which gives:

$$T(\lambda,\phi,1000) = T_m(1000) - \{\eta r(\phi-\phi_o) + \bar{T}\cos[(\lambda_o-\lambda)2\pi/L_\lambda]\cos[(\phi-\phi_o)2\pi/L_\phi]\} \quad (4.3)$$

This function proved unsatisfactory in representing intense thermal gradients in frontal zones; a nearly constant gradient over the field results when using Sanders' original function. With coastal fronts, temperature gradients of 5-10 $^{o}$C over a 20 km distance are not uncommon. To remedy this problem, a hyperbolic tangent function, dependent on a temperature difference, is utilized as a temperature correction which is added to the pattern. The correction term is given by:

$$T_{COR} = B\{TANH\{[T(\lambda,\phi,1000)-T_m(1000)]/A\}\} \quad (4.4)$$

where A = a parameter which controls the intensity of the gradient added to the field

B = amplitude of the temperature correction.

The correction function is designed to increase temperatures greater than $T_m(1000)$ and decrease temperatures less than $T_m(1000)$. Due to the nature of the hyperbolic tangent function which has its first derivative maximizing at zero, the temperature gradient (the first derivative of temperature with respect to horizontal distance) becomes greatest in the vicinity of the chosen isotherm $T_m(1000)$ where $T(\lambda,\phi,1000) - T_m(1000)$ equals zero.

The combined expression for the temperature field then becomes:

$$T_{TOTAL}(\lambda,\phi,1000) = T(\lambda,\phi,1000) + T_{COR} . \qquad (4.5)$$

Sanders' model allowed for only a north-south alignment of troughs and ridges. Therefore, his height expression had to be modified to obtain any desired orientation of the trough axis, for example, along the coast in the case of the coastal front. A tilting term (Equation 4.6) was incorporated which forces the longitude to vary as a function of latitude difference from the reference latitude:

$$\lambda_{TILT} = c(\phi-\phi_o) \qquad (4.6)$$

where c is a parameter which controls the degree of tilting, that is, the slope. Sanders' phase lag parameter ($\Delta\lambda$) is not used here since separate reference latitudes and longitudes are defined for the temperature and height fields.

To make the height gradient pattern around maxima and

minima (highs and lows) more realistic (by increasing the gradient north and decreasing the gradient south of the height center), a linear correction is added to the latitudinal factor of the height expression, where

$$\cos[(\phi-\phi_o)2\pi/L_\phi]$$

is replaced with

$$\cos[(\phi-\phi_o)2\pi/L_\phi] + D(\phi-\phi_o)$$

and D is a parameter which controls the degree of change applied to the height gradient.

Finally, a height correction dependent on the absolute difference of temperature from a given point to a chosen isotherm is added to the height field. The chosen isotherm is preferably one located in the frontal zone. Thus, the smallest corrections are being added near the front. This, in effect, forces the trough to be sharpened in the immediate vicinity of the front assuming that the patterns are matched beforehand with the temperature gradient lying in the trough of the height field. The height correction due to temperature is a quadratic function given by:

$$HTCOR = E[T_{TOTAL}(\lambda,\phi,1000)-T_{FRONT}]^2 \qquad (4.7)$$

where E = a parameter which controls the degree of sharpening of the trough, and

$T_{FRONT}$ = the mean temperature (isotherm) chosen to represent the frontal zone.

The final expression for the height field thus becomes:

$$Z(\lambda,\phi,1000) = \bar{Z}\cos\{[\lambda_o-(\lambda+\lambda_{TILT})]2\pi/L_\lambda\}\ X$$
$$\{\cos[(\phi-\phi_o)2\pi/L_\phi]+D(\phi-\phi_o)\} + HTCOR. \quad (4.8)$$

Sample plots of the resultant temperature and height fields are shown in Fig. 4.1. One should note that the surface trough through Missouri is at the warm edge of the temperature gradient; that is, along the surface cold front. Also note the production of a warm frontal trough through Michigan and Ohio.

Due to the modifications mentioned above the functions of temperature and height have become increasingly complex. Temperature is now a composite function with the hyperbolic tangent incorporated, and the height field is dependent on this temperature. Therefore, finite-differencing will be used to create the simulated fields of temperature gradients and of the wind. Finite-differencing of the resulting wind components will be used to obtain additional kinematic variables such as divergence, vorticity, and temperature advection.

## 4.2 The Simulated Wind Field

The geostrophic wind $\vec{V}_g$, which is derived directly from the height field, is the basis for the simulated wind field $\vec{V}_{SIM}$. The geostrophic wind components are defined by:

$$u_g = (-g/f)(\Delta z/\Delta y) \ ; \quad v_g = (g/f)(\Delta z/\Delta x) \quad (4.9)$$

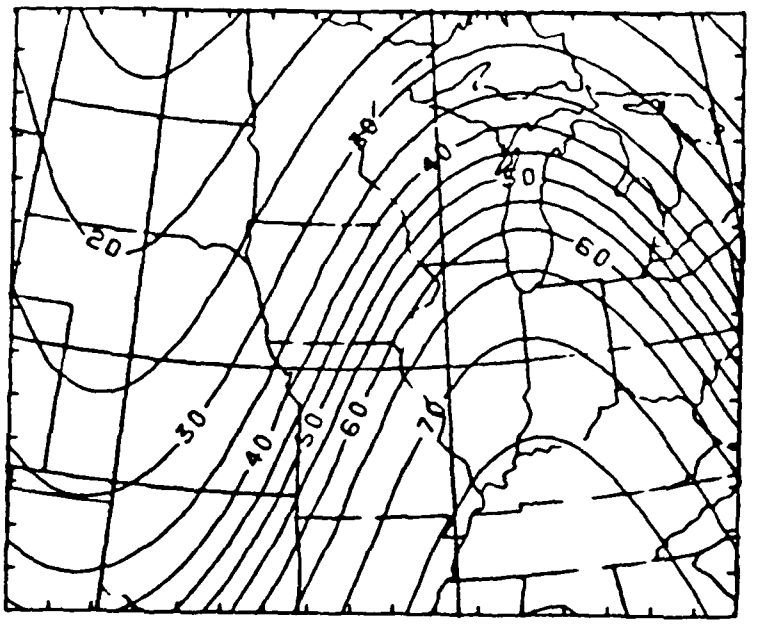


Figure 4.1a - Example of simulated 1000 mb temperature field ($^{\circ}$F).

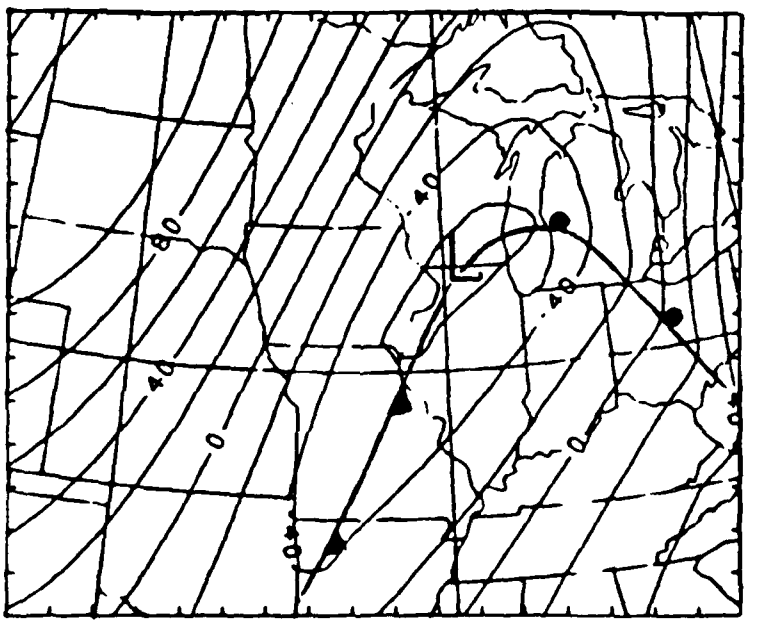


Figure 4.1b - Example of simulated 1000 mb height field (m).

where g is the acceleration of gravity

f is the Coriolis parameter

z is the 1000 mb height from the analytic field.

Friction is then added fictitiously to the geostrophic wind by utilizing a linear relation between the "actual" wind speed and the geostrophic wind speed, and by reducing the geostrophic wind direction by a constant amount ($\alpha$) and, thus, creating cross-isobaric flow toward low pressure. These alterations on the geostrophic wind are as follows:

$$|\vec{V}_{SIM}| = a\,|\vec{V}_g| \tag{4.10}$$

$$(\vec{V}_{SIM})_{DIR} = (\vec{V}_g)_{DIR} - \alpha \quad \text{if } (\vec{V}_g)_{DIR} - \alpha > 0$$

$$= (\vec{V}_g)_{DIR} - \alpha) + 360^{o} \quad \text{if } (\vec{V}_g)_{DIR} - \alpha \leq 0. \tag{4.11}$$

Baur and Phillips (1938) computed the angle ($\alpha$) between the surface wind and the geostrophic wind (land and sea), and the ratio (a) of the surface wind speed and the geostrophic wind speed for different latitudes (Table 4.1). For the test cases in this research, mean values (those for the central latitude of the grid) were chosen for all wind computations. For example, in the case of the simulated coastal front in the PAM II network, values of 43, 17, .35, and .60 were used for $\alpha_L$, $\alpha_s$, $a_L$, and $a_s$, respectively. A review of papers on east coast frontogenesis by Bosart et al. (1972) and Bosart (1975) confirmed these rough approximations.

The other contribution to the ageostrophic component of the wind which results from acceleration was also considered

Table 4.1 - The angle ($\alpha$) between the surface wind wind and the geostrophic wind, and the ratio (a) between the surface wind speed and the geostrophic wind speed for different latitudes ($\phi$), according to Baur and Philipps (1938, p. 292).

| $\phi$ | $\alpha_L$ | $\alpha_s$ | $a_L$ | $a_s$ |
|---|---|---|---|---|
| 0 | 61 | 40 | .... | .... |
| 10 | 55 | 29 | .... | .... |
| 20 | 49.5 | 23 | .... | .... |
| 30 | 45 | 19 | 0.31 | 0.56 |
| 40 | 42 | 16 | 0.38 | 0.63 |
| 50 | 39 | 14.5 | 0.42 | 0.67 |
| 60 | 37 | 13 | 0.46 | 0.70 |
| 70 | 36 | 12.5 | 0.485 | 0.715 |
| 80 | 35 | 12 | 0.495 | 0.723 |
| 90 | 35 | 12 | ..... | ..... |

for inclusion in the generation of a realistic surface wind. The ageostrophic wind $\vec{V}_a$ due to this cause was derived as follows:

$$d\vec{V}/dt = \vec{V}_g \cdot \nabla \vec{V}_g \qquad (4.12)$$

assuming the local time rate change of momentum and the vertical advection of momentum are zero, and replacing $\vec{V}$ with $\vec{V}_g$ in the horizontal advection term. The acceleration is also given by:

$$d\vec{V}/dt = -f\vec{k} \times (\vec{V}-\vec{V}_g) = -f\vec{k} \times \vec{V}_a \; ; \qquad (4.13)$$

therefore,

$$\vec{V}_a = \vec{k}/f \times (\vec{V}_g \cdot \nabla \vec{V}_g). \qquad (4.14)$$

An experiment was conducted to compare the effects of the fictitious "friction" and the ageostrophic wind $\vec{V}_a$ on the divergence field. The geostrophic wind field was derived from the 1000 mb height pattern shown in Fig. 4.1b. Then Baur and Phillips' frictional modification and $\vec{V}_a$ were added separately to this basis geostrophic wind field. From these resulting fields divergences were obtained. A comparison of grid point values revealed that the contribution to the divergence field by $\vec{V}_a$ was small compared to the contribution due to "friction".

Additional support for not incorporating $d\vec{V}/dt$ comes from a comparison of the relative magnitudes of the forces acting on the wind. The Coriolis force ,$CF=f|\vec{V}|$, based upon the frictionless wind, $\vec{V}=\vec{V}_g+\vec{V}_a$; the horizontal pressure gradient force, $HPGF=-g\nabla z$; and the accelerational force due

to the advection of the geostrophic wind (Equation 4.12) were computed over a 15X18 grid. The Coriolis force and the horizontal pressure gradient force were an order of magnitude greater than $d\vec{V}/dt$ (from Equation 4.12) over approximately 80-90% of the field. The accelerational force exceeded each of the other two forces at only 2 of the 154 test points. Furthermore, the wind field resulting from the approximation given by Baur and Phillips exhibits a very reasonable pattern and is more than sufficient for this study.

## 4.3 Sensitivity of Analyzed Fields to Error Sources

The simulated fields of temperature and height described above were used to compare the error in analyzed fields that would result from random error and from spatial data distribution and interpolation by the objective analysis scheme. The analytic meteorological fields provide a known standard for each point of the grid. To accomplish the sensitivity test the following procedure was employed:

1.) The Barnes analysis was performed on the bogus station data without random error.

2.) The analysis was repeated with random error superimposed on the data set. Random errors with mean of zero and standard deviation of 2 $^{o}$F and 3 m were added to all of the simulated observation values of temperature

and height, respectively.

3.) The two analyses were compared to the "actual" simulated grid point values, the standard, in order to calculate RMSEs.

Table 4.2 shows that the error in temperature increased slightly, while the error in height actually decreased when random errors were introduced into the fields. As the latter result was unexpected a second test was conducted with a larger standard error of height, 5 m. This led to a very slight increase in mean error. These results reveal that the analysis scheme smoothes random error very efficiently. That is, the error due to random error is practically nil compared to the error resulting from the data distribution and the analysis scheme's interpolation procedure.

Table 4.2 - Analysis error due to random error. Root-mean-square-errors are shown for analyses with and without random error using simulated fields of surface temperature and 1000 mb height.

| | Temperature | 1000 mb Height |
|---|---|---|
| Without Random Error | 1.37 $^{o}$F | 4.74 m |
| With Random Error-- (Standard deviation of error: 2 $^{o}$F and 3 m) | 1.73 | 4.66 |
| (Standard deviation of error: 5 m) | .... | 4.75 |

# CHAPTER 5

# SENSITIVITY OF ANALYZED METEOROLOGICAL FIELDS TO OBSERVATIONAL NETWORK DESIGN

## 5.1 Simulated "True" Meteorological Fields

The mathematical functions defined in the previous chapter were used to produce meteorological fields representative of a coastal front typical of the United States east coast in winter. A theoretical measure of the analysis accuracy of different observing systems can be made since the "true" values of all meteorological variables are known over the entire field. The purpose here is to determine how well the proposed PAM II network for the winter 1986 GALE project, in combination with the Barnes objective analysis scheme, describes this mesoscale weather system. Comparisons are made with four alternative observing networks to gain insight into possible improvements or changes to the proposed network design. Coastal fronts are investigated since a large portion of GALE will concern the study of these mesoscale systems and their role in cyclogenesis. Coastal fronts provide intense

temperature gradients and strong horizontal wind shears which offer a means to fully test the observing network's ability in describing related "true" meteorological fields.

Fig. 5.1 depicts the simulation of an onshore front over the coastal plains of North Carolina and South Carolina. A realistic coastal front situation is duplicated with a wedge of cold air between the front and the Appalachian Mountains; the cold air wedge is associated with the ridge of high pressure. The coastal front lies in a surface trough and is squeezed between this cold air dome and the warmer air over the ocean resulting in a temperature gradient in excess of 4 $^{o}$C over 10 km.

These patterns were produced using values (obtained from the analytic functions) on a regular rectangular grid point array with grid spacing of 12.5 km. The grid is positioned on a coordinate system which has its x-axis perpendicular, and y-axis parallel, to the coast. This allows the grid array to be aligned with the proposed PAM II network which is described in the next section.

The "true" kinematic fields, derived from the simulated wind field (Fig. 5.1c), and the temperature gradient field (magnitude) are depicted in Fig. 5.2. These patterns are representive of an intense coastal front. An axis of maximum positive vorticity, with values in excess of 30 X $10^{-5}$/s, is aligned along the frontal zone over the Carolinas. Equally strong convergence is depicted over this

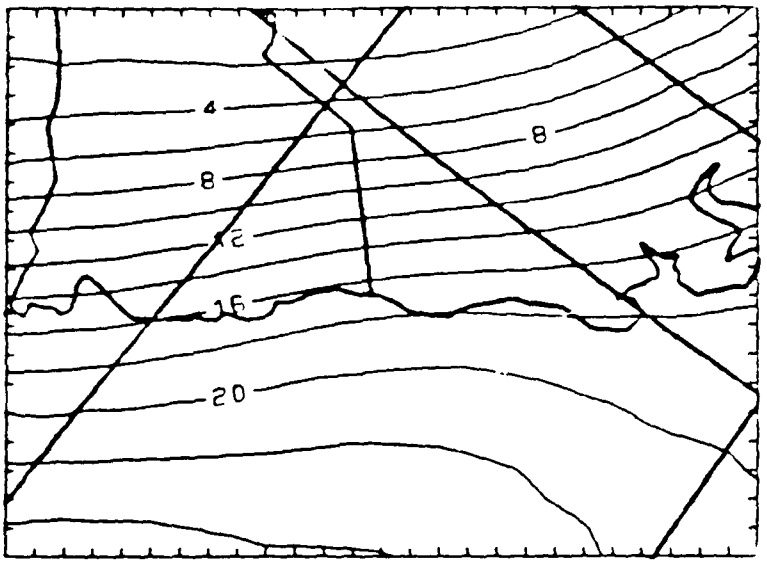


Figure 5.6a - Barnes analysis of temperature field ($^{o}C$) for simulated coastal front case.

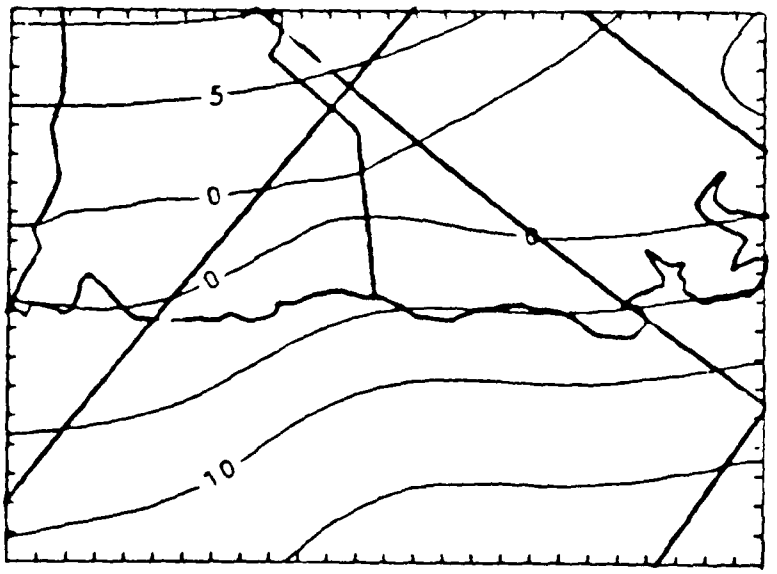


Figure 5.6b - Barnes analysis of 1000 mb height field (m).

Table 5.2 - Effects of random error. (Same as Table 5.1 except random error is added to PAM II data, with standard deviation of error of 2 $^{o}$C, 8 m, and 2 m/s for temperature, 1000 mb height, and wind components, respectively.)

| | RMSE | P. E. |
|---|---|---|
| Temperature | 2.57 | |
| 1000 mb Height | 3.91 | |
| U- component | 1.97 | 36.1 |
| V- component | 1.85 | 37.3 |
| Divergence | 4.53 | 76.9 |
| Rel. Vorticity | 5.73 | 66.7 |
| Temp. Gradient | 0.67 | 80.6 |
| Temp. Advection | 3.63 | 109.8 |
| Local Frontogenesis | 1.11 | 142.5 |

analyses confirmed the previous results in Chapters 3 and 4. Random errors had little effect on the RMSE as shown in Table 5.2; that is, the Barnes scheme effectively filtered out these errors in the data. For example, the RMSE for the temperature field increased only 0.17 $^{o}$C, from 2.40 $^{o}$C (without random error) to 2.57 $^{o}$C (with random error). The P. E.'s increased only 1-6% in the kinematic parameters.

The results in Table 5.2 reveal the magnitude of typical errors to be expected with a network such as PAM II. If the RMSE is compared to the average magnitude of the parameter over the whole objectively analyzed field, the percentage error would be unacceptably large, 100-300%. That is, the error would be 1 to 3 times as large as the analyzed value.

Fig. 5.6 shows analyses resulting from using the proposed PAM II network data with random errors incorporated. These analyses should be compared to Figs. 5.1 and 5.4. It is obvious that the network does not adequately represent the true meteorological fields. The Barnes analyzed temperature and 1000 mb height fields are grossly over-smoothed (compare Figs. 5.1a,b with Figs. 5.6a,b). The same is true in the cases of relative vorticity, divergence, and temperature gradient (Figs. 5.6d-f), for which the respective maxima are 6 X $10^{-5}$/s, -4 X $10^{-5}$/s, and 0.75 $^{o}$C/10 km. These values are only about 30% of the magnitudes of these maxima in the true fields.

Table 5.1 - Barnes analysis (using simulated PAM II data) vs. "true" field. Root-mean-square-error (RMSE) and percentage error (P. E.) are shown.

| | RMSE | P. E. |
|---|---|---|
| Temperature ($^{o}C$) | 2.40 | |
| 1000 mb Height (m) | 2.71 | |
| U- component (m/s) | 1.93 | 35.3 |
| V- component (m/s) | 1.67 | 33.6 |
| Divergence ($10^{-5}$/s) | 4.28 | 72.6 |
| Rel. Vorticity ($10^{-5}$/s) | 5.22 | 60.8 |
| Temp. Gradient ($^{o}C/10^{4}$m) | 0.64 | 77.7 |
| Temp. Advection ($^{o}C/10^{4}$s) | 3.57 | 108.1 |
| Local Frontogenesis ($^{o}C/10^{8}$ms) | 1.10 | 140.5 |

described above. However, since the "true" field, which serves as the standard, is represented by values on the finite grid, the simulated station values in the present experiments are obtained from this same set of gridded values using bilinear interpolation.

These PAM II station "data" are now objectively analyzed. Table 5.1 summarizes the RMSEs and percentage errors of the analysis based on the proposed PAM II network compared to the true field at grid points. The percentage error is given by:

$$\text{P. E.} = \text{RMSE}/[(\sum_{m=1}^{M} |V_m|)/M] \qquad (5.1)$$

and $V_m$ is the grid point value from the true meteorological field and M is the number of grid points. The RMSE of divergence over the proposed PAM II region is about 73% of the average magnitude of the divergences over the true field and similarily, about 61% for the relative vorticity. For temperature advection and local frontogenesis (local time rate of change of the magnitude of the temperature gradient) the P. E. exceeds 100%.

Random errors with means of zero and standard deviation of error of 2 $^{o}$C, 8 m, and 2 m/s for temperature, height, and u-, v- wind components, respectively, were incorporated into the PAM II station values. Such errors might simulate typical instrumental and calibration errors, as well as local exposure and siting effects. The subsequent

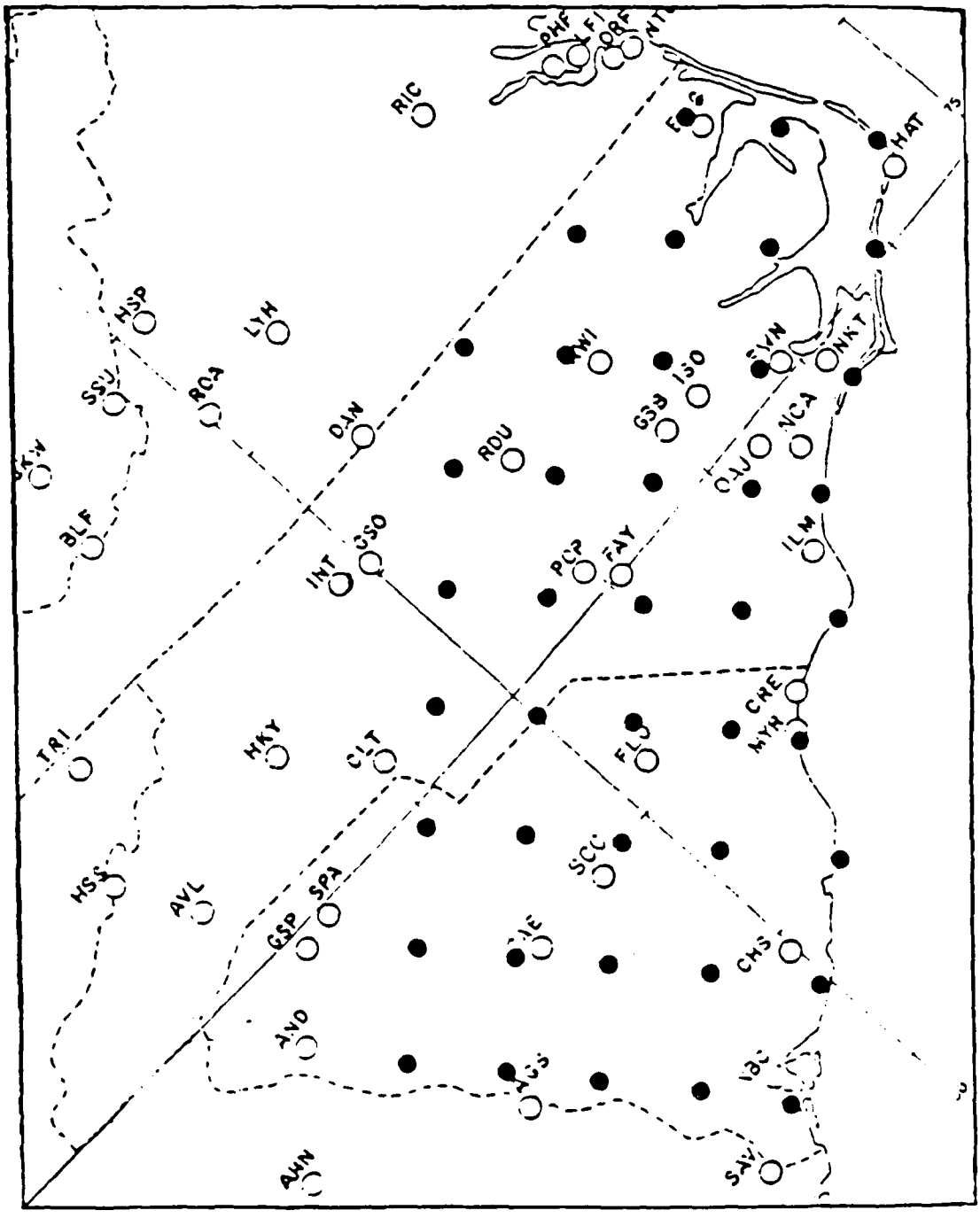


Figure 5.5 - Proposed 42-station PAM II network with approximately 60 km spacing normal to the coast and 75 km parallel to the coast.

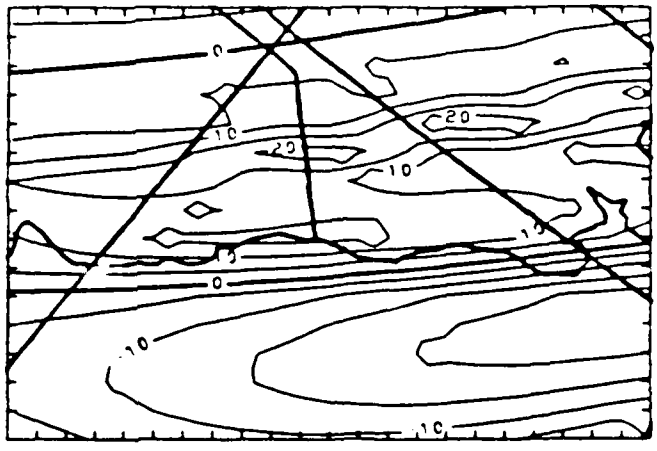


Figure 5.4a - Simulated vertical component of relative vorticity ($10^{-5}$/s) with DX = 25 km.

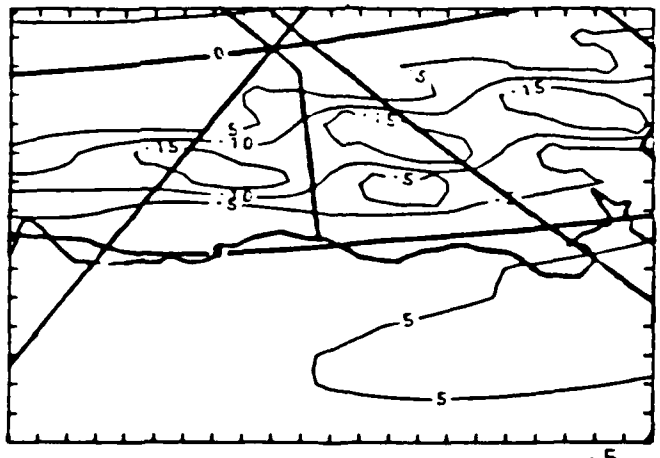


Figure 5.4b - Simulated divergence field ($10^{-5}$/s) with DX = 25 km.

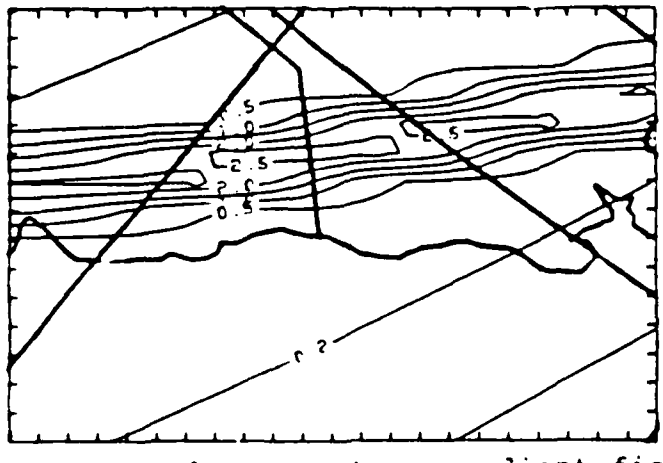


Figure 5.4c - Simulated temperature gradient field ($^{o}$C/10 km) with DX = 25 km.

dense array from the true field (DX = 12.5 km). Therefore, in order to make comparisons between the "true" fields (which serve as the standard) and the objectively analyzed data as fair as possible, the temperature and wind components from the true fields are finite-differenced using a DX of 25 km, that is, using every other grid point. This naturally decreases the magnitude of the extreme values of the various parameters in the vicinity of the front and along the coast. The patterns shown in Fig. 5.4 are used as the standard against which objectively analyzed fields are compared. The maximum values in these fields; 20 X $10^{-5}$/s for vorticity, -15 X $10^{-5}$/s for divergence, and 2.5 $^{o}$C/10 km for temperature gradient; are only 50-60% as large as the maxima in the fields where DX = 12.5 km (Fig. 5.2).

## 5.2 Experiments with the Proposed PAM II Network

The proposed PAM II network of GALE shown in Fig. 5.5 is made up of 42 land-based stations in a near-rectangular array. The values of meteorological variables (temperature, 1000 mb height, and wind components) at these stations are obtained by bilinearly interpolating the four surrounding grid point values from the true simulated field where DX = 12.5 km. The station values were also obtained directly using the mathematical functions. This gave values essentially equal to those obtained using the procedure

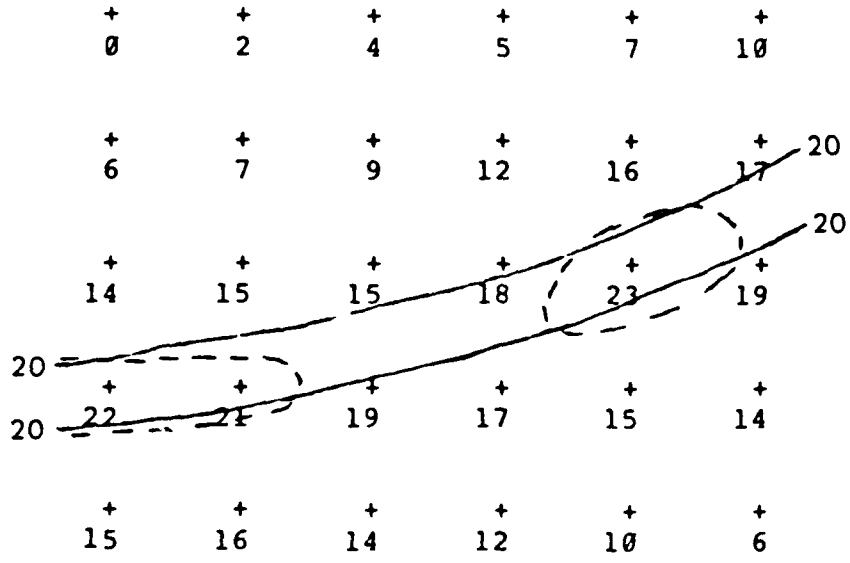


Figure 5.3 - Example of cellular pattern which results from using a finite number of grid values. Dashed lines are contours drawn when considering only grid point values. Solid lines represent the "true" continuum field.

region in Fig. 5.2b. The magnitude of the temperature gradient exceeds 4 $^{o}$C/10 km across the front (Fig. 5.2c).

The cellular patterns in these fields arise from the inherent problem of trying to represent a continuous field with a finite array of grid points. The alternative maxima and minima in the pattern produced by the contouring scheme (SURFACE II) are, as they must be, particularly prominent along the frontal zone where gradients are strongest. This problem of cellular patterns can be demonstrated with a simple example as shown in Fig. 5.3.

If the grid network was dense enough, that is, DX approaches zero, the contours would appear as the solid lines in the figure; however, since only a finite number of grid points is available the true axis of maximum values falls between the grids points and cannot be correctly represented. The result is a cellular pattern of maxima along this axis. To verify that this feature does not exist in the true continuum, the fields were reconstructed allowing the front to parallel the grid rows; with this orientation the cellular pattern was removed. In the present experiments the gridded fields with the cells are accepted as the "true" fields with the knowledge that the atmosphere is not quite correctly represented.

In the tests to be described, station values are interpolated to points of a grid which has a grid spacing of 25 km. This grid array is simply a subset set of the more

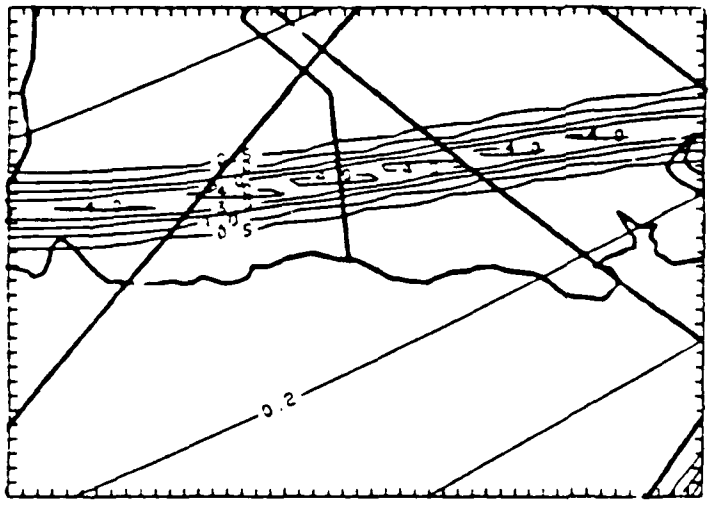


Figure 5.2c - Simulated temperature gradient field ($^{o}$C/10 km) with DX = 12.5 km.

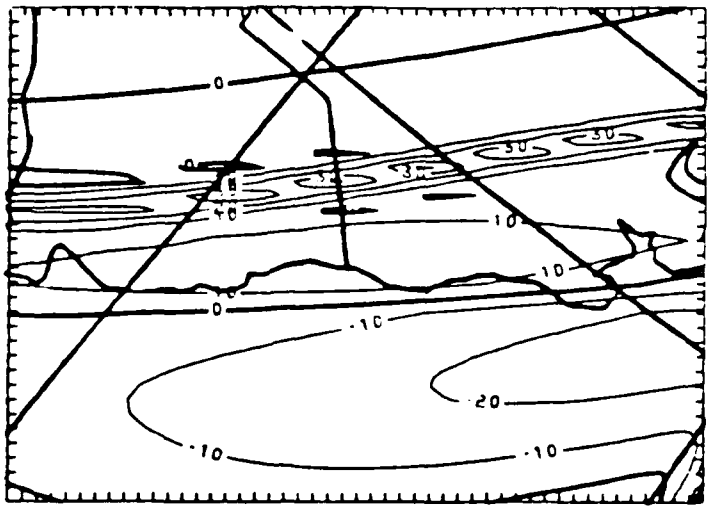


Figure 5.2a - Simulated vertical component of relative vorticity ($10^{-5}$/s) with DX = 12.5 km.

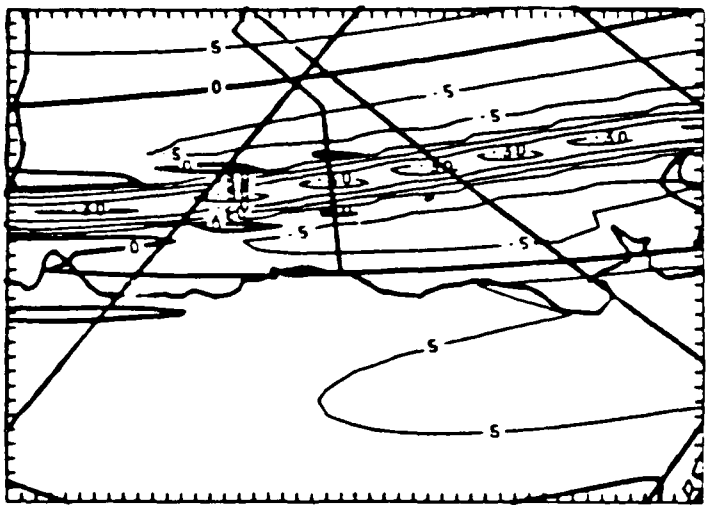


Figure 5.2b - Simulated divergence field ($10^{-5}$/s) with DX = 12.5 km.

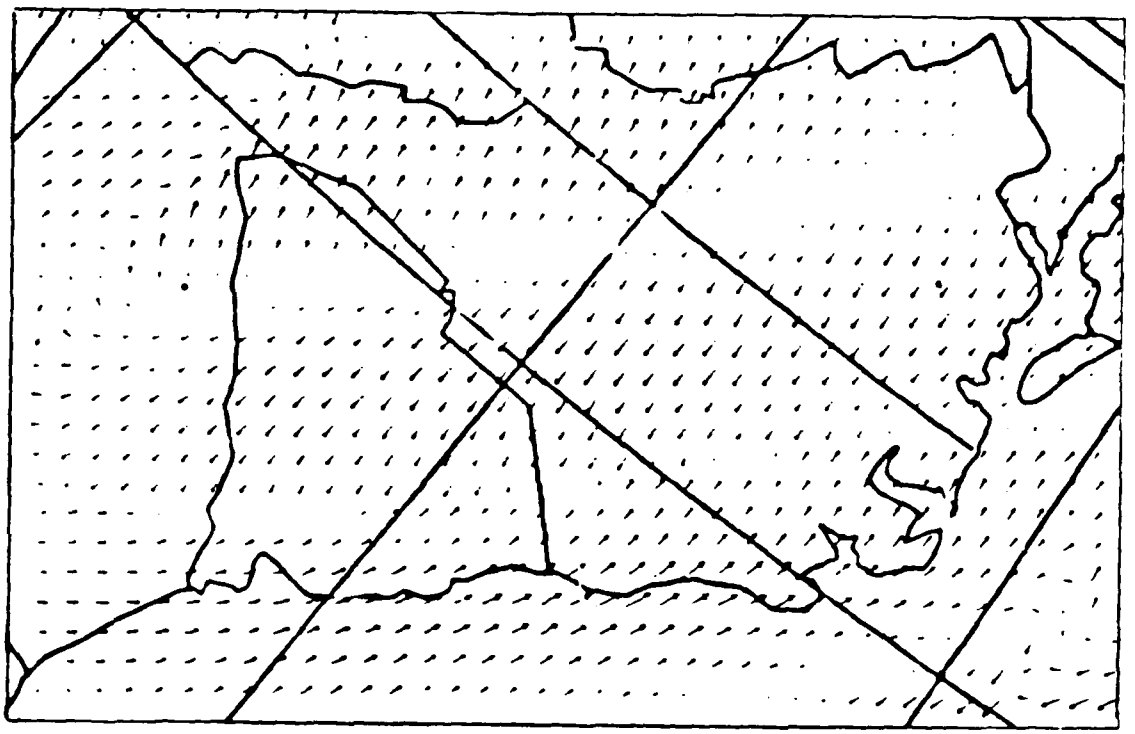

Figure 5.1c - Vector display of simulated wind field.

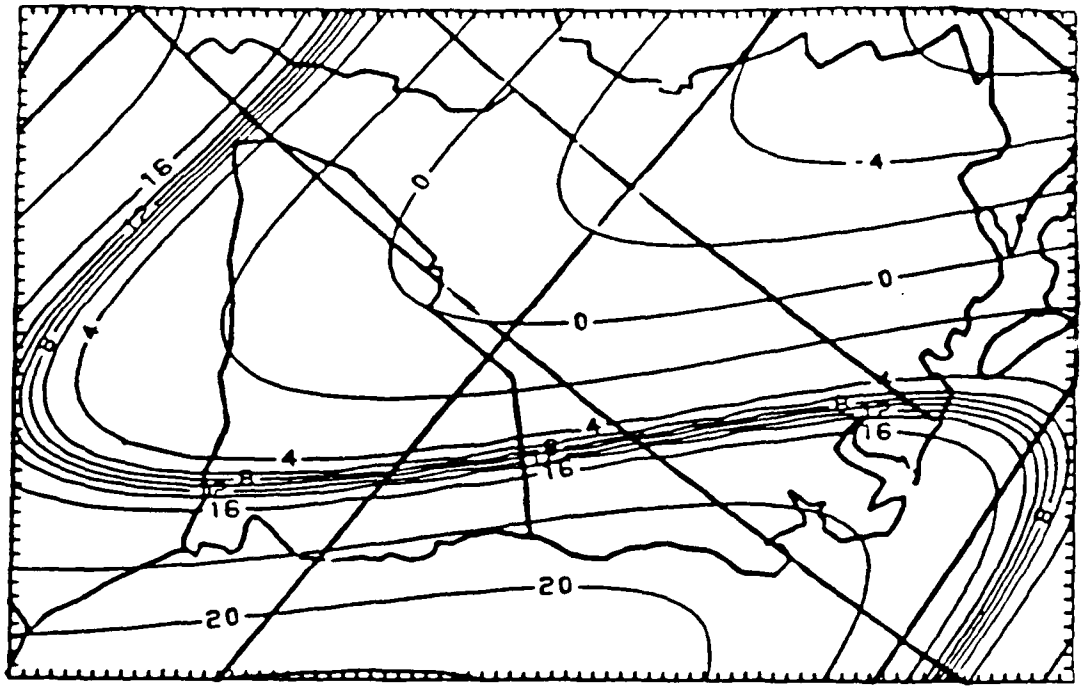


Figure 5.1a - Simulated temperature field ($^{o}$C) depicting an onshore coastal front.

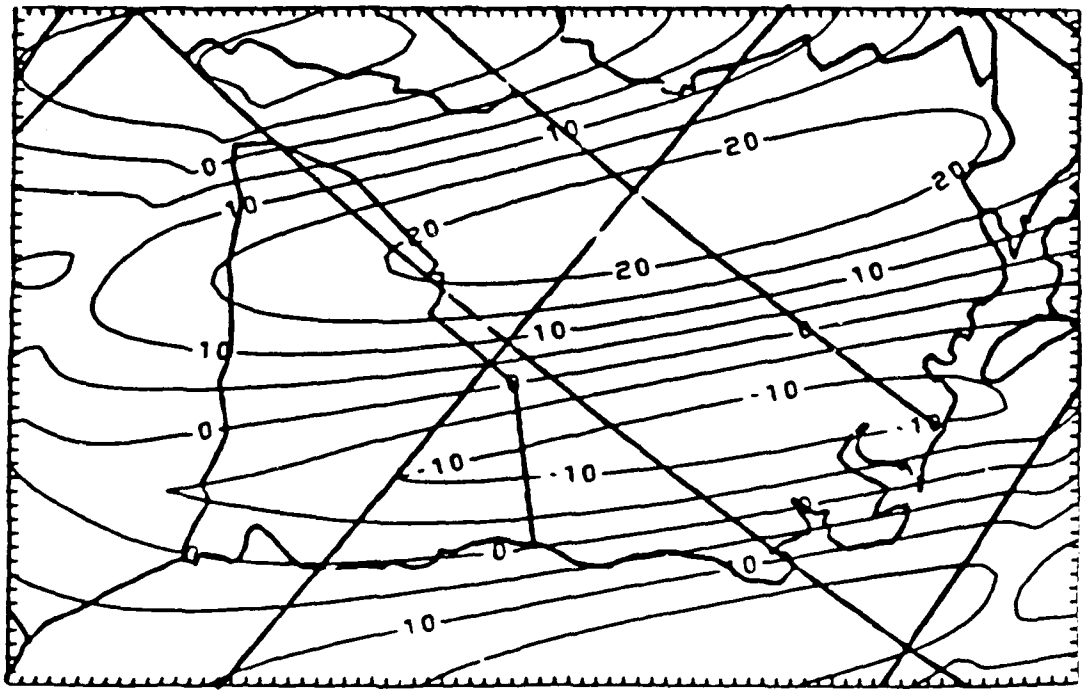


Figure 5.1b - Simulated 1000 mb height field (m).

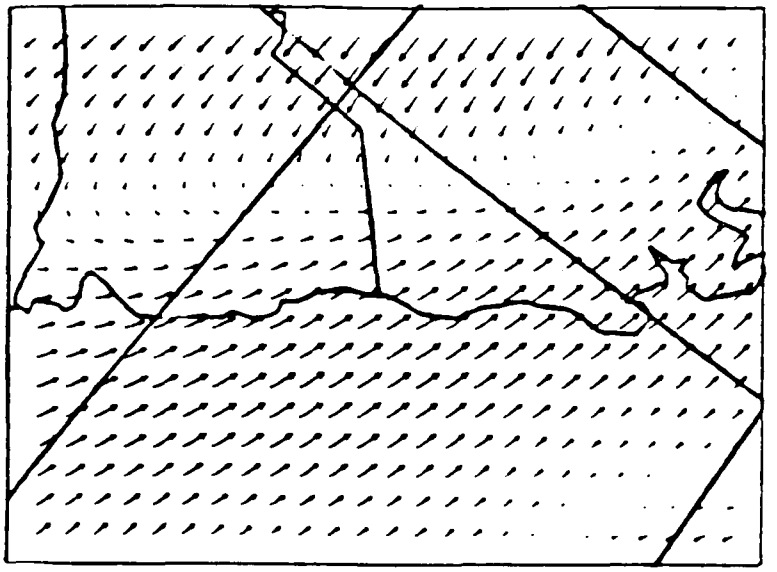

Figure 5.6c - Vector display of Barnes analysis of wind field.

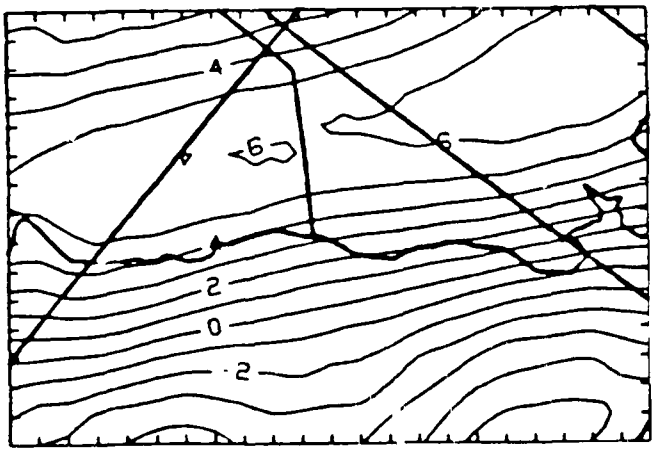


Figure 5.6d - Vertical component of relative vorticity ($10^{-5}$/s) derived from Barnes analyzed wind components.

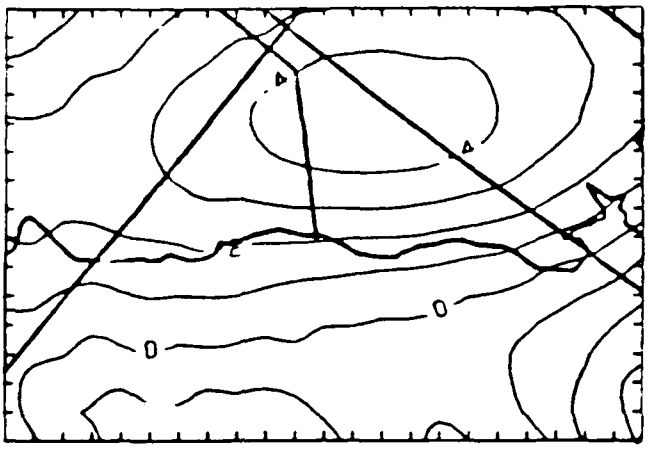


Figure 5.6e - Divergence field ($10^{-5}$/s) derived from Barnes analyzed wind components.

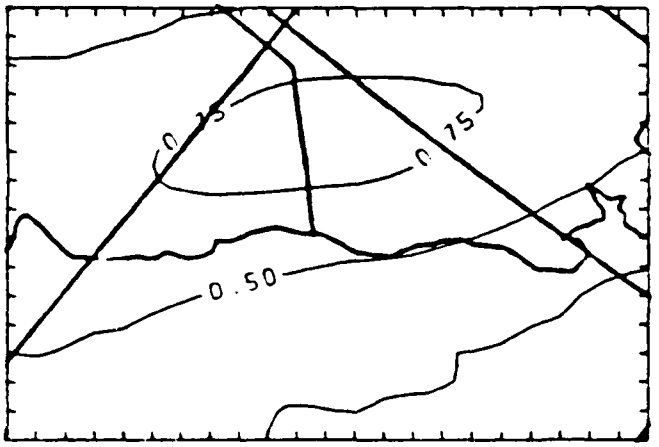


Figure 5.6f - Temperature gradient field ($^{o}$C/10 km) derived from Barnes analyzed temperature field.

## 5.3 Alternative PAM II Networks

Is the proposed PAM II network the configuration which gives the best results as regards reasonable resolution of coastal front features? To answer this question three alternative networks covering the same geographic area are investigated:

1.) 9 X 5 network - is a network configuration (shown in Fig. 5.7a) which is simply a re-arrangement of the 42 PAM II stations enhancing resolution normal to the coast (spacing of 30 km) at the expense of that along-coast (spacing of 150 km);

2.) 9 X 17 network - has approximately four times the number of stations as in the present PAM II network; that is, the station density is doubled in both directions resulting in station spacings of 30 km normal to the coast and 37.5 km parallel to the coast (Fig. 5.7b);

3.) 5 X 5 network - contains approximately one-half the number of PAM II stations (spacing of 60 km normal to and 150 km parallel to the coast) and is more nearly compatible with the spacing of the regular hourly reporting stations (Fig. 5.7c).

In addition, a network of 34 regular hourly reporting stations (National Weather Service, Federal Aviation Administration, and military stations) overlying approximately the same area was subjected to the same test

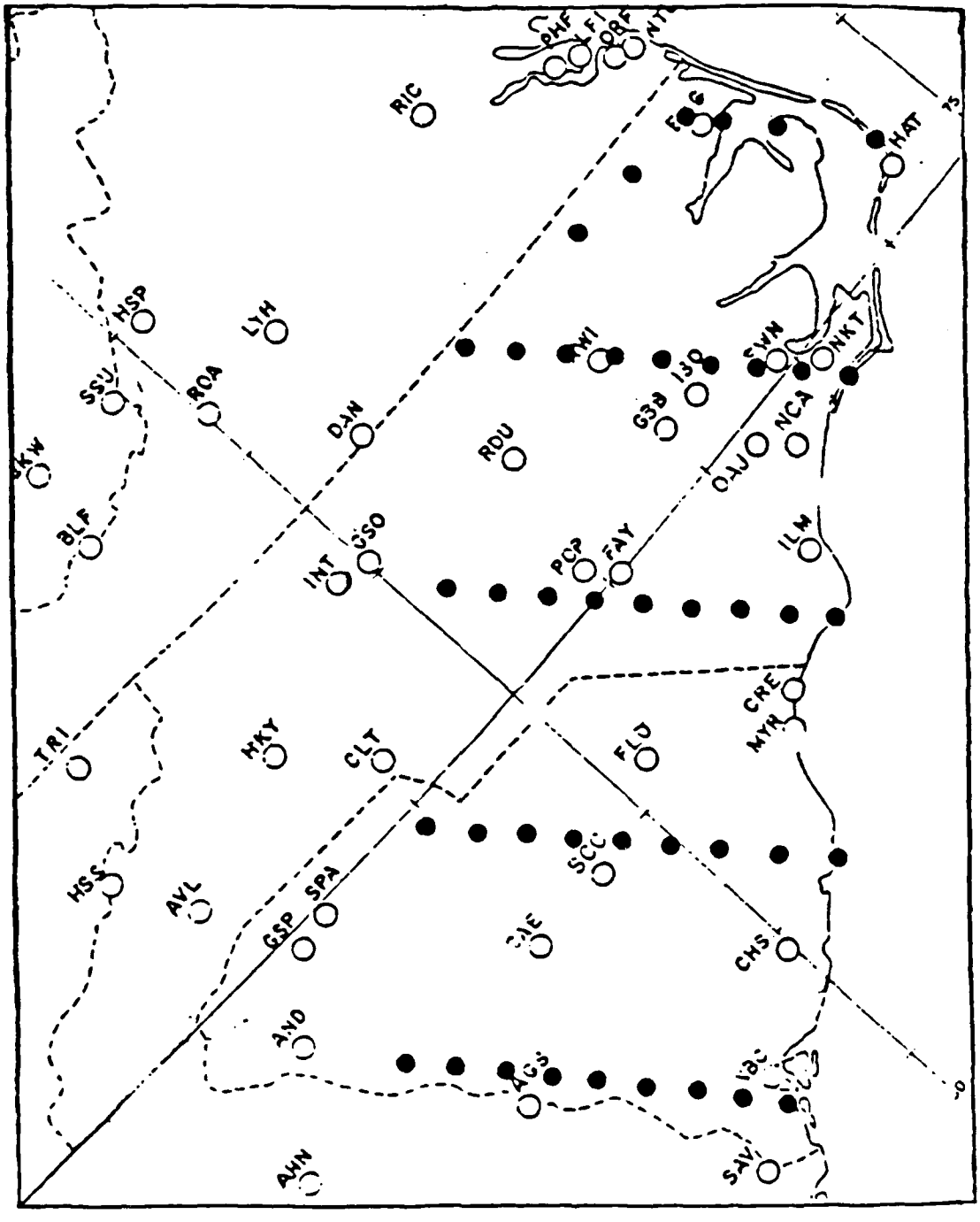


Figure 5.7a - A possible "9 X 5" PAM II observation network.

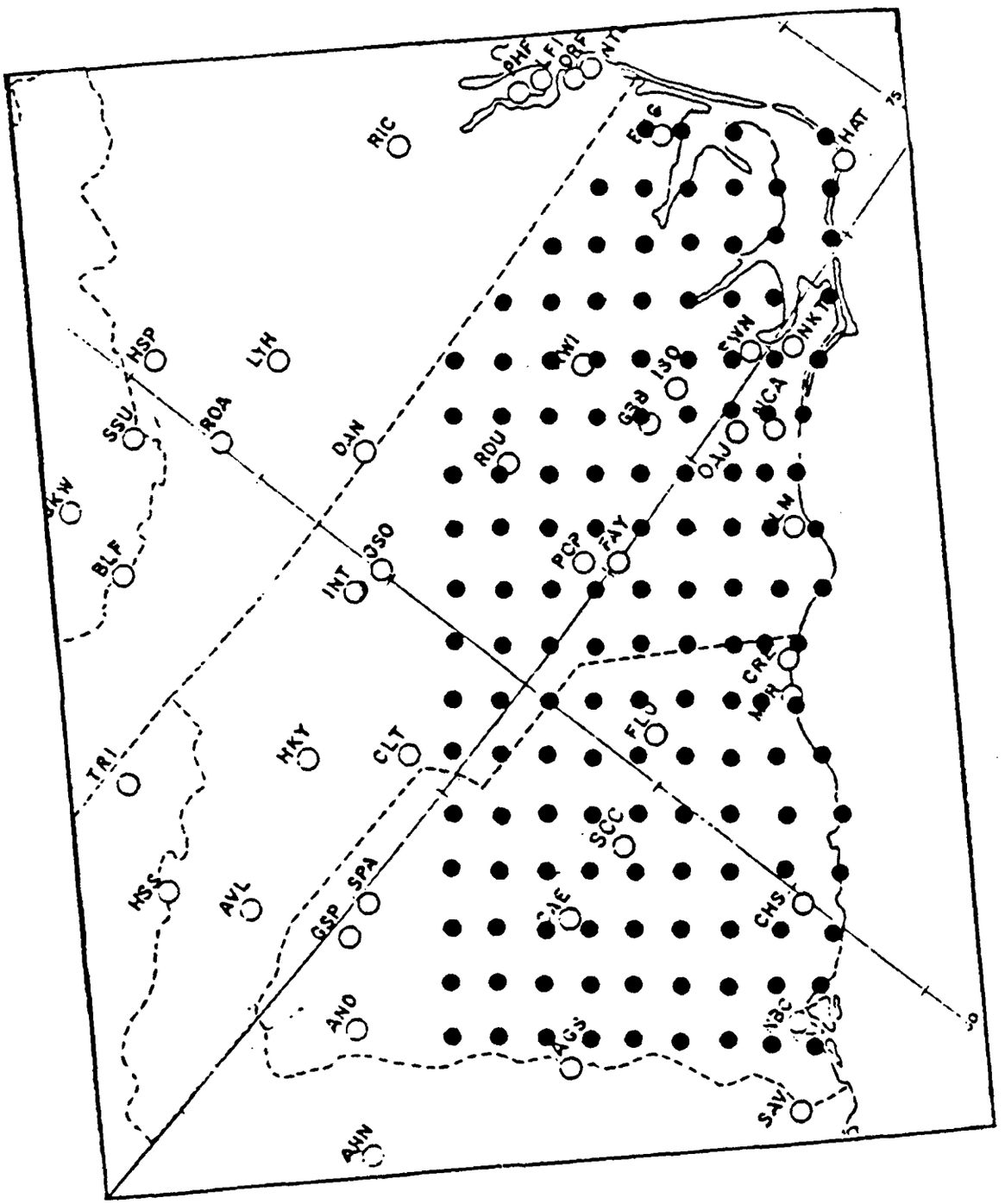


Figure 5.7b - A possible "9 X 17" PAM II observation network.

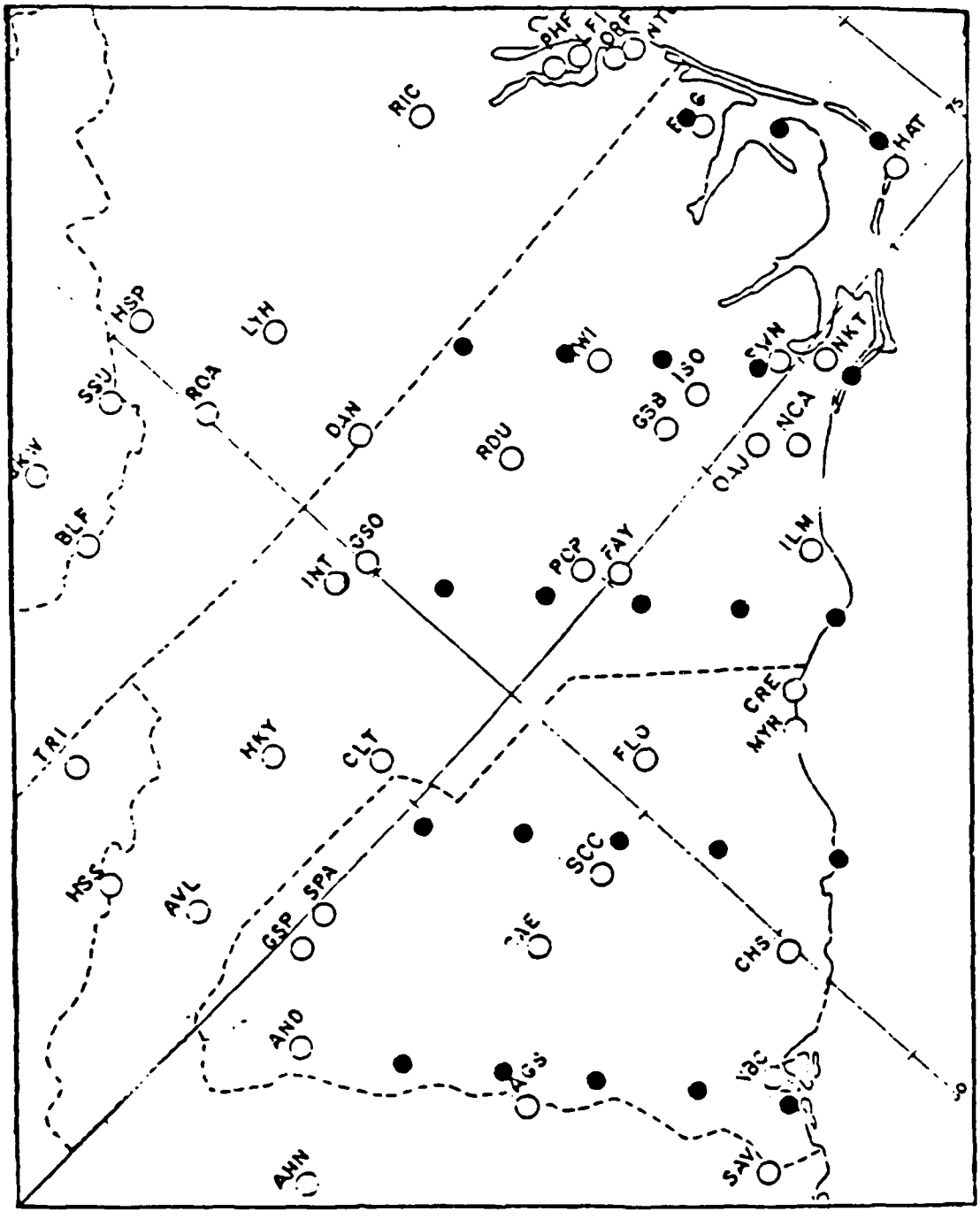


Figure 5.7c - A possible "5 X 5" PAM II observation network.

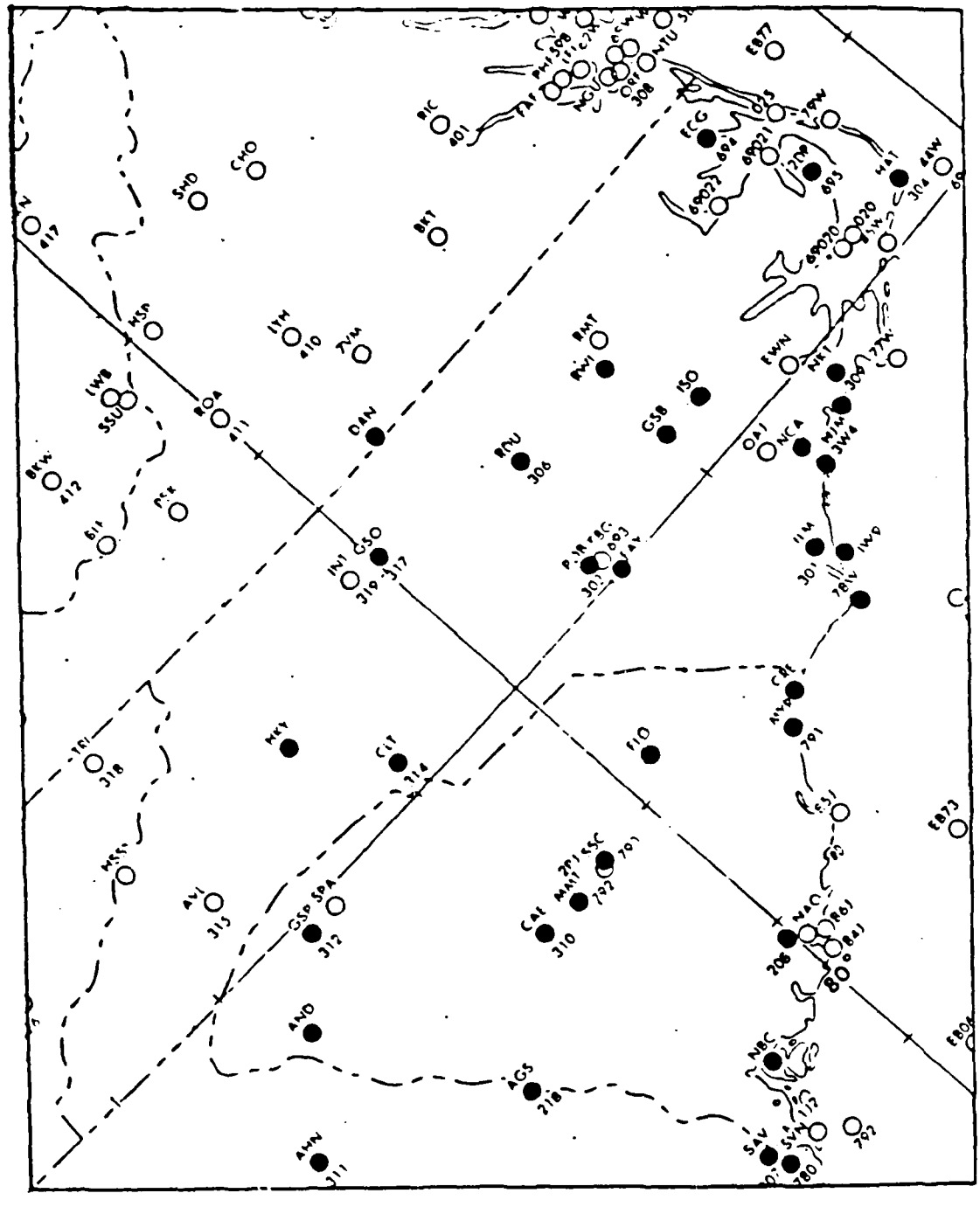


Figure 5.7d - Regular hourly reporting station network.

(Fig. 5.7d).

These tests were made with random error added to the station values. A range of weight parameters ,$k_o$'s, were used in the tests because the different station densities warranted it. However, to make equitable comparisons between networks, results using the same $k_o$ are also compared.

A summary of the results of these several experiments are outlined in Table 5.3. It is apparent that the RMSE decreased with increasing station density. The least dense network, 5 X 5 network (23 stations) produced the largest errors with a mean error of 17.41 m for the 1000 mb height and 12.60 m/s for the u- component of the wind ($k_o$ = 200). The 9 X 17 configuration generally produced the smallest errors which were about 10% less than those generated using the proposed PAM II (5 X 9) network. For example, in the relative vorticity field an error of 5.11 X $10^{-5}$/s occurred with the 9 X 17 network and 5.73 X $10^{-5}$/s with the proposed PAM II. However, this is only a slight improvement when one considers that the station density was approximately quadrupled. Since the scale of the mesoscale features of the front are small compared to the average station spacing, the 9 X 17 network fails to significantly improve the analysis accuracy.

The re-arrangement of the proposed PAM II network into the 9 X 5 configuration increased the station density across

Table 5.3 - Comparison of observation networks. Summary of results: Root-mean-square-errors and percentage errors for surface temperature ($^{o}$C), 1000 mb height (m), wind components (m/s), divergence and relative vorticity ($10^{-5}$/s) with random error incorporated into data.

| | | 9 X 17 | | 9 X 5 | | (Proposed PAM II) 5 X 9 | | 5 X 5 | | Regular Hourly Network | |
|---|---|---|---|---|---|---|---|---|---|---|---|
| | | RMSE | P. E. | RMSE | P. E. | RMSE | P. E. | RMSE | P. E. | RMSE | P. E. |
| | Temperature | 2.47 | ..... | 2.02 | ..... | 2.57 | ..... | | | | |
| | 1000 mb Height | 3.56 | ..... | 5.07 | ..... | 3.91 | ..... | | | | |
| $k_o$=50 | U- component | 1.79 | 32.8 | 2.21 | 40.4 | 1.97 | 36.1 | | | | |
| | V- component | 1.69 | 34.1 | 1.42 | 28.6 | 1.85 | 37.3 | | | | |
| | Divergence | 4.33 | 73.5 | 4.61 | 78.2 | 4.53 | 76.9 | | | | |
| | Rel. Vorticity | 5.11 | 59.5 | 5.71 | 66.5 | 5.73 | 66.7 | | | | |
| | Temperature | 3.53 | ..... | 3.33 | ..... | 3.74 | ..... | 14.14 | ..... | 6.56 | ..... |
| | 1000 mb Height | 5.10 | ..... | 6.27 | ..... | 5.91 | ..... | 17.41 | ..... | 6.91 | ..... |
| $k_o$=200 | U- component | 2.96 | 54.3 | 3.68 | 67.5 | 3.41 | 62.5 | 9.11 | 167.0 | 5.21 | 95.5 |
| | V- component | 2.63 | 53.0 | 2.68 | 54.0 | 3.05 | 61.6 | 12.60 | 254.2 | 5.55 | 112.0 |
| | Divergence | 6.36 | 107.9 | 6.28 | 106.4 | 6.02 | 102.0 | 7.14 | 121.1 | 7.38 | 125.1 |
| | Rel. Vorticity | 6.75 | 78.6 | 7.23 | 84.1 | 7.48 | 87.1 | 8.89 | 103.5 | 8.81 | 102.5 |
| | Temperature | | | | | 4.68 | ..... | 13.98 | ..... | 7.27 | ..... |
| | 1000 mb Height | | | | | 7.19 | ..... | 17.28 | ..... | 7.28 | ..... |
| $k_o$=400 | U- component | | | | | 4.44 | 81.3 | 8.33 | 152.6 | 5.71 | 104.6 |
| | V- component | | | | | 3.83 | 77.2 | 11.79 | 237.8 | 6.05 | 122.1 |
| | Divergence | | | | | 6.92 | 117.2 | 7.12 | 120.7 | 7.68 | 130.1 |
| | Rel. Vorticity | | | | | 8.47 | 98.6 | 8.97 | 104.4 | 9.49 | 110.5 |

the front and decreased the density along the frontal boundary. As a result, the analysis accuracy changed little; the mean errors approximately equaled those of the PAM II network (Table 5.3). While offering a potential monetary savings through requiring fewer observational stations, the 5 X 5 network proved to be significantly less accurate than the proposed PAM II network.

The proposed PAM II system was more accurate than the regular hourly reporting network. This is partly due to the greater station density of the PAM II network (42 vs. 34 stations), and partly to the irregular spatial distribution of the hourly reporting stations. The PAM II system has another important advantage over the regular reporting stations which was not simulated in this study. PAM II stations will be able to make observations at small time intervals (every five minutes). This increased time resolution will provide data which can be filtered with respect to time to remove high frequency noise and make the analysis more reliable. The regular reporting stations only make one observation per hour which, in most cases, will not be representative of the whole hour. Furthermore, the greater time resolution of the PAM II network will permit time-to-space conversion of observations and thus enhance spatial resolution if features move with known velocity through the observation network.

The results in Table 5.3 show that the mean error

generally decreased as the weight parameter decreased. This is expected when error-free data taken from the true field are analyzed. However, even with random errors in the data the RMSE can continue to decrease with decreasing $k_o$ because the component of the RMSE independent of random error dominates over the component of the RMSE due to random error. The former component, which is due to the nearly unresolvable short-wave features in the frontal zone, is so large that the incorporation of random errors has little effect on the noise level of the field. Therefore, increased noise in the field due to random error does not become the dominate feature and allow an optimum $k_o$ to be obtained, as was the case with the optimum weight parameter test in Chapter 3.

The above experiments were repeated for each station network without incorporating random error. Table 5.4 shows RMSEs calculated when these analyses are compared to the true fields. The analyses of the uncontaminated data fields lead to results similar to those in Table 5.3. Again, the mean error is correlated to station density, with the proposed PAM II network having errors less than the 5 X 5 and hourly reporting station networks, approximately equal to the 9 X 5 network, and slightly greater than the 9 X 17 network.

Table 5.4 - Comparison of observation networks without random error and $k_o$ = 200. Root-mean-square-errors and percentage errors for surface temperature ($^{o}$C), 1000 mb height (m), wind components (m/s), divergence and relative vorticity ($10^{-5}$/s).

| | 9 X 17 | | 9 X 5 | | (Proposed PAM II) 5 X 9 | | 5 X 5 | | Regular Hourly Network | |
|---|---|---|---|---|---|---|---|---|---|---|
| | RMSE | P. E. | RMSE | P. E. | RMSE | P. E. | RMSE | P. E. | RMSE | P. E. |
| Temperature | 3.45 | ..... | 3.60 | ..... | 3.68 | ..... | 8.37 | ..... | 4.29 | ..... |
| 1000 mb Height | 4.91 | ..... | 5.93 | ..... | 6.00 | ..... | 12.56 | ..... | 6.52 | ..... |
| U- Component | 2.99 | 54.7 | 3.35 | 61.3 | 3.41 | 62.5 | 5.58 | 102.2 | 3.58 | 65.6 |
| V- Component | 2.56 | 51.6 | 2.97 | 60.0 | 3.01 | 60.8 | 5.83 | 117.7 | 3.39 | 68.5 |
| Divergence | 6.26 | 106.1 | 6.05 | 102.5 | 6.09 | 103.2 | 7.15 | 121.1 | 6.25 | 105.9 |
| Rel. Vorticity | 6.57 | 76.6 | 7.23 | 84.1 | 7.13 | 83.1 | 9.68 | 112.8 | 6.63 | 77.2 |

# CHAPTER 6

## SUMMARY AND CONCLUSIONS

The process of objective analysis has been investigated in this study using the interpolation technique devised by Barnes (1973). A method of determining optimum weight parameters for the Barnes objective analysis scheme has been tested. The "missing station" technique enabled a single value of weight parameter to yield a minimum mean error in the analysis since the datum at the point of interpolation was not in the data set utilized by the analysis scheme. This method seems more appropriate than those employed by Barnes (1973) and Koch et al. (1981). The tests described in Chapter 3 showed that the weight parameter that resulted in a total response of 0.936 for the minimum resolvable 2 $\Delta n$ wave yielded the optimum results. However, these tests were performed with only one case; several are needed to obtain more conclusive results. Therefore, it is suggested that a test similar to the one described be conducted prior to extensive analyses to obtain the appropriate weight parameter for a given data distribution and meteorological setting.

Analyses produced on a grid mesh with grid spacing approximately equal to the average station spacing were compatible with those produced on the grid with spacing of about one-half the initial grid. Therefore, when costs are considered, it is more practical to use a DX > $\Delta n/2$.

The Barnes objective analysis scheme proved generally more accurate than detailed hand analyses of kinematic fields such as divergence and vorticity. These comparisons were made using the average of several subjective analyses performed by experienced analysts as the standard.

Edge effects are quite pronounced; that is, the Barnes interpolation became unreliable near the edge of the data domain. Extrapolation into data void regions gave increasingly erroneous results. This mimics similar difficulties in subjective analyses.

When data sets were artificially contaminated with random errors of a magnitude which simulates typical instrument and exposure errors, the final analysis revealed no deterimental effects. That is, the Barnes scheme effectively smoothed (filtered) the random error from the analysis. As a result, most of the error in the analysis can be attributed to the application of the analysis scheme (interpolation) and to the limitations of the observing network, for example, its configuration, station density, and frequency of observation. However, different results could be obtained if the random errors added to the field

AD-A156 911 APPLICATION OF AN OBJECTIVE ANALYSIS SCHEME TO MESOSCALE OBSERVATIONAL NETWORK DESIGN(U) AIR FORCE INST OF TECH WRIGHT-PATTERSON AFB OH D E HARMS 1985 2/2

UNCLASSIFIED AFIT/CI/NR-85-43T F/G 12/1 NL

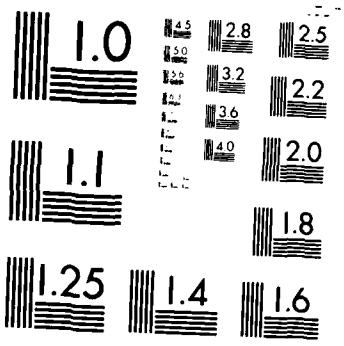

are much larger than values used in this study. After the incorporation of an extremely high degree of artificial error, the process of removing that error would inevitably remove much of the texture of the original data field.

A mathematical model has been developed which enables fronts with extremely intense gradients to be constructed. Through the simulation of a typical east coast coastal front, the analysis accuracies of the proposed (5 X 9) PAM II network for the 1986 GALE project and four alternative networks were tested. In addition, an a priori estimate of typical errors, which results from utilizing the PAM II network and the Barnes objective analysis as a tool to reconstruct meteorological fields, has been accomplished.

These experiments show that errors are unacceptably large in the kinematic fields on the mesoscale, with RMSEs approaching 100% of the true values, and even greater in temperature advection and local frontogenesis. Therefore, one is fortunate just to achieve the correct sign (+ or -) of the divergence and vorticity when attempting to reconstruct the mesoscale pattern with the present PAM II design.

Though being poor in its description of the "true" fields, the proposed PAM II network is nearly as good as a 9 X 17 configuration which halves the station spacing. The more dense 9 X 17 network did not provide a significant improvement, probably because the scale of the features in

the fields was so small that the increase in station density had little effect; that is, the stations were still too far apart to adequately resolve the intense gradients. The PAM II network (42 stations) produced somewhat better results than the regular reporting hourly network (34 stations). However, the potential exists that the analysis accuracy of the proposed PAM II network can be significantly better than that of the regular station network since the PAM II stations will be able to make, record, and transmit observations almost continuously. Time-to-space conversion of observations can be helpful if the coastal front, or any feature, is moving and is approximately in steady-state. This would, in effect, increase the data density considerably. Also automobile transverses across the front, not simulated in this study, could possibly improve the analysis accuracy.

In order to fully depict mesoscale features, the results of experiments in this research indicate that spatial separation of observation sites should be on the order of the wavelength (or less) of the mesoscale feature under consideration. That is, for an observational network to describe the intense temperature gradients and wind shears typical of a coastal front and which occur in a narrow zone of 5 to 20 km in width, observations are needed approximately every 5 to 10 km, or even less.

# LIST OF REFERENCES


Barnes, S. L., 1964: A technique for maximizing details in numerical weather map analysis. J. Appl. Meteor. , 3, 396-409.

_____, 1973: Mesoscale objective map analysis using weighted time-series observations. NOAA Technical Memorandum ERL NSSL-62 , Norman, OK, 60 pp.

Baur, F., and H. Phillips, 1938: Untersuchungen der Reibung bei Luftstromungen uber dem Meer. Ann. Hydrogr. u. mar. Meteor. , 66, 279-296.

Bengtsson, L., and N. Gustavsson, 1971: An experiment in the assimilation of data in dynamical analysis. Tellus , 23, 328-336.

Bergthórsson, P., and B. Döös, 1955: Numerical weather map analysis. Tellus , 7, 329-340.

Bosart, L. F., C. J. Vaudo and J. H. Helsdon, Jr., 1972: Coastal frontogenesis. J. Appl. Meteor. , 11, 1236-1258.

Bosa t, L. F., 1975: New England coastal frontogenesis. Quart. J. Royal Meteor. Soc. , 101, 957-978.

Cressman, G. P., 1959: An operational objective analysis system. Mon. Wea. Rev. , 87, 367-374.

Eddy, A., 1967: The statistical objective analysis of scalar data fields. J. Appl. Meteor. , 6, 597-609.

Gandin, L. S., 1963: Objective Analy is of Meteorological Fields . Gidrometeor. Izdatel'stvo, Leningrad (Israel Program for Scientific Translations, Jerusalem, 1965, 242 pp.

Gilchrist, B., and G. P. Cressman, 1954: An experiment in objective analysis. Tellus , 6, 309-318.

Inman, R. L., 1970: Operational objective analysis schemes at the National Severe Storms Forecast Center. Technical Circular No. 10 NSSL , Norman, OK, 50 pp.

Koch, S. E., M. des Jardins and P. J. Kocin, 1981: The Gempak Barnes objective analysis scheme. NASA Technical Memorandum 83851 , NASA/GLAS, Greenbelt, MD 20771, 56 pp.

_____, 1983: An interactive Barnes objective map analysis scheme for use with satellite and conventional data. J. Clim. Appl. Meteor. , 22, 1487-1503.

Koehler, T. L., 1979: A case study of height and temperature analyses derived from nimbus-6 satellite soundings on a fine mesh model grid . PHD Thesis, Univ. of Wisconsin - Madison, p. 107-161.

McPherson, R. D., 1975: Progress, problems and prospects in meteorological data assimilation. Bull. Amer. Meteor. Soc. , 56, 1154-1166.

Otto-Bliesner, B., D. P. Baumhefner and T. W. Schlatter, 1977: A comparison of several meteorological analysis schemes over a data-rich region. Mon. Wea. Rev. , 105, 1083-1091.

Panofsky, H. A., 1949: Objective weather map analysis. J. Meteor. , 6, 386-392.

Penn, S., B. Kunkel and W. D. Mount, 1963: On objective analysis of continuous and discontinuous parameters. J. Appl. Meteor. , 2, 345-350.

Rutherford, I. D., 1972: Data assimilation by statistical interpolation of forecast error fields. J. Atmos. Sci. , 29, 809-815.

_____, 1973: Experiments on the updating of P. E. forecasts with real wind and geopotential data. Preprints Third Conf. on Probability and Statistics in Atmospheric Science , 19-22 June 1973, Boulder, CO, Amer. Meteor. Soc., 198-201.

Sanders, F., 1971: Analytic solutions of the nonlinear omega and vorticity equation for a structurally simple model of disturbances in the baroclinic westerlies. Mon. Wea. Rev. , 99, 393-407.

Sasaki, Y., 1958: An objective analysis based on the variational method. J. Meteor. Soc. Japan , 36, 77-88.

_____, 1970: Some basic formalisms in numerical variational analysis. Mon. Wea. Rev. , 98, 875-883.

Schlatter, T. W., G. W. Branstator and L. G. Thiel, 1976: Testing a global multivariate statistical objective analysis scheme with observed data. Mon. Wea. Rev. , 104, 765-783.

Seaman, R. S., 1977: Absolute and differential accuracy of analyses achievable with specified observational network characteristics. Mon. Wea. Rev. , 105, 1211-1222.

Shapiro, M. A., and J. T. Hastings, 1973: Objective cross-section analyses by Hermite polynomial interpolation on isentropic surfaces. J. Appl. Meteor. , 12, 753-762.

Thiebaux, H. J., 1975: Experiments with correlation representations for objective analysis. Mon. Wea. Rev. , 103, 617-627.